ELSEVIER

Journal of Quantitative Spectroscopy & Radiative Transfer 109 (2008) 1641–1666

Journal of Quantitative Spectroscopy & Radiative Transfer

www.elsevier.com/locate/jqsrt

Elliptic PDE formulation and boundary conditions of the spherical harmonics method of arbitrary order for general three-dimensional geometries

Michael F. Modest*, Jun Yang

Department of Mechanical and Nuclear Engineering, The Pennsylvania State University, University Park, PA 16802, USA

Received 3 May 2007; received in revised form 3 December 2007; accepted 17 December 2007

Abstract

The inherent complexity of the radiative transfer equation makes the exact treatment of radiative heat transfer impossible even for idealized situations and simple boundary conditions. Therefore, a wide variety of efficient solution methods have been developed for the RTE. Among these solution methods the spherical harmonics method, the moment method, and the discrete ordinates method provide means to obtain higher-order approximate solutions to the equation of radiative transfer. Although the assembly of the governing equations for the spherical harmonics method requires tedious algebra, their final form promises great accuracy for any given order, since it is a spectral method (rather than finite difference/finite volume in the case of discrete ordinates). In this study, a new methodology outlined in a previous paper on the spherical harmonics method (P_N) is further developed. The new methodology employs successive elimination of spherical harmonic tensors, thus reducing the number of first-order partial differential equations needed to be solved simultaneously by previous P_N approximations ($=(N+1)^2$). The result is a relatively small set ($=N(N+1)/2$) of second-order, elliptic partial differential equations, which can be solved with standard PDE solution packages. General boundary conditions and supplementary conditions using rotation of spherical harmonics in terms of local coordinates are formulated for the general P_N approximation for arbitrary three-dimensional geometries. Accuracy of the P_N approximation can be further improved by applying the "modified differential approximation" approach first developed for the P_1-approximation. Numerical computations are carried out with the P_3 approximation for several new two-dimensional problems with emitting, absorbing, and scattering media. Results are compared to Monte Carlo solutions and discrete ordinates simulations and a discussion of ray effects and false scattering is provided.

Keywords: Radiative transfer equation; Spherical harmonics; High-order; Three-dimensional

1. Introduction

The radiative transfer equation (RTE) is an integro-differential equation in five independent variables (three in space and two in direction), which is exceedingly difficult to solve. Exact analytical solutions to the RTE

*Corresponding author. Fax: +1 814 863 4848.
E-mail address: mfm6@psu.edu (M.F. Modest).

0022-4073/$ - see front matter © 2007 Elsevier Ltd. All rights reserved.
doi:10.1016/j.jqsrt.2007.12.018

Nomenclature

A_i	phase function coefficients
$D^n_{mm'}$	Wigner function
I	radiative Intensity
I^m_n	intensity coefficient function
J	spherical harmonics series
$\mathscr{L}$	differential operator
L	slab thickness
ll1, **ll2**, **ls1**, **ls2**	coefficient tensors
$\hat{n}$	unit normal vector
P^m_n	associated Legendre polynomial
q_n	net radiative flux (normal to surface)
R	direction vector length
$\hat{s}, \vec{s}$	(unit) direction vector
sl1, **sl2**, **ss1**, **ss2**	coefficient tensors
Y^m_n	spherical harmonic

Greek symbols

α, γ	property parameters
α, β, γ	Euler rotation angles
β	extinction coefficient
δ	surface rotation angle
$\boldsymbol{\delta_{ij}}$	single-term unit tensor, Eq. (23)
Δ	rotation tensor
ε	surface emittance
κ	absorption coefficient
θ	polar angle
μ	$\equiv \cos\theta$
σ_s	scattering coefficient
τ	optical coordinate
Φ	scattering phase function
ω	single scattering albedo
Ω	solid angle

Subscripts

b	blackbody
m, w	medium and wall emission contributions in MDA
s	surface

exist only for a very few simple situations, such as one-dimensional plane-parallel media without scattering. Accurate numerical solutions for more complicated geometries or scenarios are also very difficult to obtain. Several approximate methods have been developed over time. Among these approximate methods the *spherical harmonics method* (SHM), the *discrete ordinates method* (DOM) or the *finite volume method* (FVM), the *zonal method*, and the *Monte Carlo method* have been used most frequently [1]. The *zonal method* enjoyed early popularity, but its solution is expensive (inversion of full matrices) and it cannot treat anisotropic scattering, and it is rarely used today. Both the SHM and the DOM/FVM approximate the directional variation of the radiative intensity rather than its spatial behavior. However, the underlying approaches to

represent the directional dependence of radiative intensity for SHM and DOM/FVM are quite different. The DOM employs a discrete representation of the directional variation with integrals over total solid angle 4π obtained via numerical quadrature, while the SHM captures the directional distribution of intensity by expressing it into a series of spherical harmonics. The DOM/FVM method is relatively simple to implement, but has several drawbacks, such as the fact that an iterative solution is required in the presence of scattering media or reflecting surfaces. In addition, its convergence is known to slow down for optically thick media. Furthermore, DOM may suffer ray effects and possibly false scattering due to its angular discretization [2]. The SHM has several advantages over other approximate methods: first, it converts the integro-differential RTE into relatively simple partial differential equations, similar to DOM/FVM. In our preliminary study [3] we have shown that a set of coupled second order PDEs can be extracted from these equations, which can be solved by using standard PDE solver packages. Secondly, in this method the spatial and directional dependencies are completely decoupled, allowing independent choices for spatial and directional accuracy, without suffering detrimental ray effects.

On the other hand, like all methods, the SHM also has a number of drawbacks. The lowest-order P_N approximation, the P_1-approximation, has enjoyed great popularity because of its relative simplicity and compatibility with standard methods for the solution of the energy equation [1]. However, the P_1-approximation performs poorly in the optically thin limit and other nonisotropic radiative intensity fields. Mathematical complexity increases rapidly if higher-order P_N approximations for multi-dimensional geometry are desired, which is probably responsible for the fact that its development lags behind that for the DOM/FVM. The fact that in the SHM intensity is expressed in terms of spherical harmonics makes it difficult to accurately represent directionally strongly anisotropic intensity as encountered, for example, near emitting walls and/or in optically thin media. For the P_1-approximation this can be largely mitigated by using the modified differential approximation (MDA) approach of Olfe [4] and Modest [5].

A number of higher-order P_N approximations have been formulated for specific (usually one-dimensional) geometries [6–10] and for limited three-dimensional applications [11,12], as recently reviewed by Yang and Modest [3]. In Yang and Modest's preliminary work presented at Eurotherm 78 [3] a methodology was outlined, which decomposes the RTE into $N(N+1)/2$ coupled second-order elliptic partial differential equations for a given odd order N, allowing for variable properties and arbitrary three-dimensional geometries.

It is the purpose of the present paper to extend the preliminary work of Yang and Modest (i) by presenting the necessary mathematical details, (ii) extending the methodology so that higher-order approximations (P_5, P_7, etc.) can be extracted directly, (iii) by generalizing and directly evaluating the necessary boundary conditions for arbitrary three-dimensional geometries, (iv) by showing that the MDA approach can be applied to all orders of P_N, making it vastly more accurate, and (v) by presenting a couple of new examples to demonstrate the accuracy of P_3 and modified-P_3 as compared to the DOM/FVM, both being solved with commercial codes (FlexPDE [13] and Fluent [14]).

2. Mathematical formulation

We have shown in our preliminary work [3] how the spherical harmonics approach can be formulated for general three-dimensional media with spatially varying properties, and how—after eliminating odd-numbered harmonics—this can be reduced to a set of $N(N+1)/2$ coupled elliptic PDEs, as given by Eq. (16) below. For convenience of the reader this development is repeated here, giving same additional mathematical details. The development is then continued to actually formulate these $N(N+1)/2$ equations in terms of spatial coefficients I_n^m of even spherical harmonics (n even). Similarly, boundary condition for the general P_N-method, first formulated for the configuration considered in [3] will be generalized by the rotation of harmonics to arbitrary orientations. Finally, it will be demonstrated how the MDA approach of Olfe [4] and Modest [5] can be generalized and integrated into higher order P_N-schemes.

2.1. Notation and properties of spherical harmonics

For a given location $\vec{\tau}$ using optical coordinates based on the extinction coefficient β, i.e., $\mathrm{d}\vec{\tau} = \beta\,\mathrm{d}\vec{x}$, where $\vec{x}$ is the position vector, let $\vec{s}$ be a vector of arbitrary magnitude R originating at $\vec{\tau}$, such that $\vec{s} = R\hat{s}$, with $\hat{s}$ being

a unit direction vector. Following Davison [11], we may express the intensity field $I(\vec{\tau},\hat{s})$ in terms of an infinite series:

$$I(\vec{\tau},\hat{s}) = \frac{1}{4\pi}\sum_{n}[(2n+1)J_n(\vec{\tau},\vec{s})]_{R=1}, \tag{1}$$

where

$$J_n = \frac{1}{2n+1}\sum_{m=-n}^{n} I_n^m(\vec{\tau})\,Y_n^m(\vec{s}). \tag{2}$$

In Eq. (2) the $I_n^m(\vec{\tau})$ are location-dependent coefficient functions associated with a given spherical harmonic $Y_n^m(\vec{s})$, while directional dependency of the intensity field is resolved in terms of a series of integral-degree real spherical harmonics defined as [15]

$$Y_n^m(R,\theta,\phi) = \begin{cases} R^n\cos(m\phi)P_n^m(\cos\theta) & \text{for } m\geqslant 0,\\ R^n\sin(m\phi)P_n^m(\cos\theta) & \text{for } m<0,\end{cases} \tag{3}$$

and $P_n^m(\cos\theta)$ are *associated Legendre polynomials*, given by

$$P_n^m(\mu) = (-1)^m\frac{(1-\mu^2)^{|m|/2}}{2^n n!}\frac{d^{n+|m|}}{d^{n+|m|}\mu}(\mu^2-1)^n. \tag{4}$$

Here θ and ϕ are the polar and azimuthal angles defining the direction of the unit vector $\hat{s}$. Based on the orthogonality of spherical harmonics over the solid angle of 4π, we have

$$\int_{4\pi}[Y_n^m(R,\theta,\phi)]_{R=1}^2\,\mathrm{d}\Omega = \frac{(n+|m|)!}{(n-|m|)!}\frac{2\pi(1+\delta_{m,0})}{(2n+1)}, \tag{5}$$

where $\delta_{m,0}$ is Kronecker's delta.

2.2. RTE transformation

The general equation of radiative transfer has the form [1]

$$\hat{s}\cdot\nabla_\tau I + I = (1-\omega)I_\mathrm{b} + \frac{\omega}{4\pi}\int_{4\pi} I(\hat{s}')\Phi(\hat{s}\cdot\hat{s}')\,\mathrm{d}\Omega', \tag{6}$$

where ω is the single scattering albedo. Augmentation of intensity due to in-scattering is calculated by the last term in the above equation, where Φ is the scattering phase function and describes the probability that a ray from direction $\hat{s}'$ will be scattered into a certain direction, $\hat{s}$. The intensity gradient, ∇_τ, along direction $\hat{s}$ is written in terms of nondimensional optical coordinates with the extinction coefficient β introduced for Eq. (1).

For an order of N ($N\geqslant 1$) approximation, $I_n^m = 0$ for $n>N$. Substituting Eq. (1) into the RTE, we find

$$\left[\sum_{n=0}^{N}(2n+1)\hat{s}\cdot\nabla_\tau J_n\right]_{R=1} = -\left[\sum_{n=0}^{N}(2n+1)J_n\right]_{R=1} + (1-\omega)4\pi I_\mathrm{b} + \frac{\omega}{4\pi}\int_{4\pi}\left[\sum_{n=0}^{N}(2n+1)J_n(\tau,\hat{s}')\right]_{R=1}\Phi(\hat{s}\cdot\hat{s}')\,\mathrm{d}\Omega'. \tag{7}$$

For anisotropic scattering the scattering phase function Φ may be expanded into Legendre polynomials as [1]

$$\begin{aligned}\Phi(\hat{s}\cdot\hat{s}') &= 1+\sum_{j=1}^{N}A_jP_j(\hat{s}\cdot\hat{s}')\\ &= 1+\sum_{j=1}^{N}A_jP_j(\mu)P_j(\mu') + 2\sum_{j=1}^{N}\sum_{i=1}^{j}\frac{(j-i)!}{(j+i)!}A_jP_j^i(\mu)P_j^i(\mu')\cos\left[i(\phi-\phi')\right],\end{aligned} \tag{8}$$

where $\mu \equiv \cos\theta$, and A_j are the coefficients for higher-order approximations of anisotropic scattering. The order of A_j is limited to N, because the orthogonality of spherical harmonics truncates to order N upon integration of the in-scattering term. The in-scattering source term in Eq. (7) can be further simplified using Eq. (2). The resulting simple expression follows from the orthogonality of both Legendre polynomials and associated Legendre polynomials as

$$\frac{\omega}{4\pi}\int_{4\pi}\left[\sum_{n=0}^{N}(2n+1)J_n(\vec{\tau},\hat{s}')\right]_{R=1}\Phi(\hat{s}\cdot\hat{s}')\,\mathrm{d}\Omega' = \left[\omega\sum_{n=0}^{N}A_nJ_n(\vec{\tau},\hat{s})\right]_{R=1}. \tag{9}$$

The operator $\hat{s}\cdot\nabla_\tau J_n$ in Eq. (7) can be written as a combination of different orders of spherical harmonics as [11]

$$[\hat{s}\cdot\nabla_\tau J_n]_{R=1} = \left[\hat{s}\cdot\nabla_\tau J_n - \frac{R^2}{2n+1}\nabla_s\cdot\nabla_\tau J_n\right]_{R=1} + \left[\frac{1}{2n+1}\nabla_s\cdot\nabla_\tau J_n\right]_{R=1}, \tag{10}$$

where the first term on the right is a spherical harmonic of order $n+1$ and the second is one of order $n-1$. Substituting Eq. (10) into Eq. (7) and collecting spherical harmonics of order n, we obtain

$$\nabla_s\cdot\nabla_\tau J_{n+1} + (2n+1)J_n + (2n-1)\hat{s}\cdot\nabla_\tau J_{n-1} - R^2\nabla_s\cdot\nabla_\tau J_{n-1} = 4\pi(1-\omega)I_b\delta_{n,0} + \omega A_nJ_n. \tag{11}$$

For convenience a property parameter α_n can be defined as

$$\alpha_n = (2n+1) - \omega A_n, \tag{12}$$

which may be a function of spatial location. Eq. (11) then becomes

$$\nabla_s\cdot\nabla_\tau J_{n+1} + \alpha_nJ_n + [(2n-1)\hat{s} - R^2\nabla_s]\cdot\nabla_\tau J_{n-1} = 4\pi(1-\omega)I_b\delta_{n,0}. \tag{13}$$

Since we have collected the nth order harmonics, Eq. (13) constitutes a set of $2n+1$ independent PDEs of first order in space. To construct elliptic second-order PDEs (and to reduce the number of PDEs), every odd order J_n is expressed from Eq. (13) as

$$J_n = -\frac{1}{\alpha_n}(\nabla_s\cdot\nabla_\tau J_{n+1} + \nabla_\tau\cdot\mathscr{L}_{n-1}J_{n-1}) \quad \text{for } n = 1,3,5,\ldots,N, \tag{14}$$

where $\mathscr{L}_{n-1} = [(2n-1)\hat{s} - R^2\nabla_s]$ represents the operator in Eq. (13). Thus, the transformed RTE becomes, for even orders of $n = 0,2,4,\ldots,N-1$,

$$\begin{aligned}&-\nabla_s\cdot\nabla_\tau\left[\frac{1}{\alpha_{n+1}}\nabla_\tau\cdot(\nabla_sJ_{n+2} + \mathscr{L}_nJ_n)\right]\\ &\quad= -\alpha_nJ_n + \nabla_\tau\cdot\mathscr{L}_{n-1}\left[\frac{1}{\alpha_{n-1}}\nabla_\tau\cdot(\nabla_sJ_n + \mathscr{L}_{n-2}J_{n-2})\right] + 4\pi(1-\omega)I_b\delta_{n,0}.\end{aligned} \tag{15}$$

As given by Eq. (2), the spatial dependence of the J_n can be separated from its directional dependence; similarly, spatial derivatives can be isolated from directional derivatives. Thus, Eq. (15) can be rearranged as

$$\begin{aligned}&-\left[\nabla_\tau\left(\frac{1}{\alpha_{n+1}}\nabla_\tau\right)\right]^{\mathrm{T}} : \nabla_s\nabla_sJ_{n+2} - \left[\nabla_\tau\left(\frac{1}{\alpha_{n-1}}\nabla_\tau\right)\right]^{\mathrm{T}} : \mathscr{L}_{n-1}\mathscr{L}_{n-2}J_{n-2}\\ &\quad-\left\{\left[\nabla_\tau\left(\frac{1}{\alpha_{n+1}}\nabla_\tau\right)\right]^{\mathrm{T}} : \nabla_s\mathscr{L}_n - \alpha_n + \left[\nabla_\tau\left(\frac{1}{\alpha_{n-1}}\nabla_\tau\right)\right]^{\mathrm{T}} : \mathscr{L}_{n-1}\nabla_s\right\}J_n = 4\pi(1-\omega)I_b\delta_{n,0},\end{aligned} \tag{16}$$

where operators $\nabla_s\nabla_s$, $\nabla_s\mathscr{L}$, $\mathscr{L}\nabla_s$, and $\mathscr{L}\mathscr{L}$ are simply different combinations of the two basic operators ∇_s and $\mathscr{L}$. To obtain an expression for these two basic operators first-order directional derivatives must be carried out in the appropriate form. Since the directional components of J_n are best expressed in terms of R, $\mu = \cos\theta$ and ϕ, derivatives in terms of the direction cosines (s_x, s_y, s_z) for ∇_s are transformed by applying the

chain rule as

$$\frac{\partial}{\partial s_x} = \cos\phi\sin\theta\frac{\partial}{\partial R} - \frac{\mu\cos\phi\sin\theta}{R}\frac{\partial}{\partial\mu} - \frac{\sin\phi}{R\sin\theta}\frac{\partial}{\partial\phi}, \tag{17a}$$

$$\frac{\partial}{\partial s_y} = \sin\phi\sin\theta\frac{\partial}{\partial R} - \frac{\mu\sin\phi\sin\theta}{R}\frac{\partial}{\partial\mu} + \frac{\cos\phi}{R\sin\theta}\frac{\partial}{\partial\phi}, \tag{17b}$$

$$\frac{\partial}{\partial s_z} = \mu\frac{\partial}{\partial R} + \frac{1-\mu^2}{R}\frac{\partial}{\partial\mu}, \tag{17c}$$

where it has been assumed that the polar angle θ is measured from the z-axis, and the azimuthal angle ϕ from the x-axis in the x–y-plane. After rather tedious algebra, the three components of the operator ∇_s on a given spherical harmonic Y_n^m are obtained as

$$\begin{aligned}
&\frac{\partial Y_n^m}{\partial s_x} = \frac{1}{2}Y_{n-1}^{m+1} - \frac{1}{2}\pi_2(n+m-1)Y_{n-1}^{m-1}, && m>0,\\
&\frac{\partial Y_n^m}{\partial s_x} = Y_{n-1}^1, && m=0,\\
&\frac{\partial Y_n^{-m}}{\partial s_x} = \frac{1}{2}Y_{n-1}^{-(m+1)} - \frac{1}{2}\pi_2(n+m-1)(1-\delta_{m,1})Y_{n-1}^{-(m-1)}, && m>0, \qquad (18a)\\
&\frac{\partial Y_n^m}{\partial s_y} = \frac{1}{2}Y_{n-1}^{-(m+1)} + \frac{1}{2}\pi_2(n+m-1)(1-\delta_{m,1})Y_{n-1}^{-(m-1)}, && m>0,\\
&\frac{\partial Y_n^m}{\partial s_y} = Y_{n-1}^{-1}, && m=0,\\
&\frac{\partial Y_n^{-m}}{\partial s_y} = -\frac{1}{2}Y_{n-1}^{m+1} - \frac{1}{2}\pi_2(n+m-1)Y_{n-1}^{m-1}, && m>0, \qquad (18b)\\
&\frac{\partial Y_n^{\pm m}}{\partial s_z} = (n+m)Y_{n-1}^{\pm m}, && m\geqslant 0 \qquad (18c)
\end{aligned}$$

where, for later convenience, we have chosen to separate the Y_n^m and Y_n^{-m} groups (making m always a positive integer), and introduced the integer function

$$\pi_k(n) = \prod_{j=0}^{k-1}(n+j), \tag{19}$$

e.g., $\pi_2(n) = n(n+1)$, etc. Similarly, $\mathscr{L}_n Y_n^m$ can be shown to result in

$$\begin{aligned}
&\mathscr{L}_{n,x}Y_n^m = -\tfrac{1}{2}Y_{n+1}^{m+1} + \tfrac{1}{2}\pi_2(n-m+1)Y_{n+1}^{m-1}, && m>0,\\
&\mathscr{L}_{n,x}Y_n^m = -Y_{n+1}^1, && m=0,\\
&\mathscr{L}_{n,x}Y_n^{-m} = -\tfrac{1}{2}Y_{n+1}^{-(m+1)} + \tfrac{1}{2}\pi_2(n-m+1)(1-\delta_{m,1})Y_{n+1}^{-(m-1)}, && m>0, \qquad (20a)\\
&\mathscr{L}_{n,y}Y_n^m = -\tfrac{1}{2}Y_{n+1}^{-(m+1)} - \tfrac{1}{2}\pi_2(n-m+1)(1-\delta_{m,1})Y_{n+1}^{-(m-1)}, && m>0,\\
&\mathscr{L}_{n,y}Y_n^m = -Y_{n+1}^{-1}, && m=0,\\
&\mathscr{L}_{n,y}Y_n^{-m} = \tfrac{1}{2}Y_{n+1}^{m+1} + \tfrac{1}{2}\pi_2(n-m+1)Y_{n+1}^{m-1}, && m>0, \qquad (20b)\\
&\mathscr{L}_{n,z}Y_n^{\pm m} = (n-m+1)Y_{n+1}^{\pm m}, && m\geqslant 0. \qquad (20c)
\end{aligned}$$

It can be seen from Eqs. (18) through (20) that the ∇_s operator decreases the order of spherical harmonics by one, while operator $\mathscr{L}$ increases the order by one. Thus, in Eq. (16) all four terms involved with double operators $\nabla_s\nabla_s$, $\nabla_s\mathscr{L}$, $\mathscr{L}\nabla_s$, and $\mathscr{L}\mathscr{L}$ give a total of $2n+1$ independent spherical harmonics of order n. Consequently, $(2n+1)$ independent second-order PDEs can be constructed by collecting spatial derivatives of the I_n^m, corresponding to the coefficients of each independent spherical harmonic.

The double directional operators may be evaluated and terms collected as shown here for $\nabla_s\nabla_s$:

$$\nabla_s\nabla_s(2n+5)J_{n+2} = \sum_{m''=-(n+2)}^{n+2} I_{n+2}^{m''} \sum_{m'=-2}^{2} (\mathbf{ss1}_n^{m''-m',m'}\ Y_n^{m''-m'} + \mathbf{ss2}_n^{m''-m',m'}\ Y_n^{-(m''-m')}), \tag{21}$$

where $\mathbf{ss1}_n^{m,m'}$ and $\mathbf{ss2}_n^{m,m'}$ each are 5 $(-2\leqslant m'\leqslant +2)$ 3×3 tensors in s_x-s_y-s_z-space, with n and m as parameters. Note that the **ss1** and **ss2** are nonzero only for such values that the m in Y_n^m is $m\geqslant 0$ when zero is approached from positive values, and $m\leqslant -1$ when zero is approached from the negative side. Reordering Eq. (21) leads to

$$\begin{aligned}
\nabla_s\nabla_s(2n+5)J_{n+2} &= I_{n+2}^0\left\{\sum_{m'=-2}^{0} \mathbf{ss1}_n^{-m',m'}\ Y_n^{-m'} + \sum_{m'=-2}^{-1} \mathbf{ss2}_n^{-m',m'}\ Y_n^{m'}\right\} \\
&\quad + \sum_{m''=1}^{n+2}\left\{ I_{n+2}^{m''}\left(\sum_{m'=-2}^{m''} \mathbf{ss1}_n^{m''-m',m'}\ Y_n^{m''-m'} + \sum_{m'=-2}^{m''-1} \mathbf{ss2}_n^{m''-m',m'}\ Y_n^{-(m''-m')}\right)\right. \\
&\quad \left. + I_{n+2}^{-m''}\left(\sum_{m'=-2}^{m''-1} \mathbf{ss1}_n^{m'-m'',-m'}\ Y_n^{m'-m''} + \sum_{m'=-2}^{m''} \mathbf{ss2}_n^{m'-m'',-m'}\ Y_n^{-(m'-m'')}\right)\right\} \\
&= I_{n+2}^0\left\{\mathbf{ss1}_n^{0,0} + 2\sum_{m=1}^{2}(\mathbf{ss1}_n^{m,-m}\ Y_n^m + \mathbf{ss2}_n^{m,-m}\ Y_n^{-m})\right\} \\
&\quad + \sum_{m=0}^{n}\sum_{m'=\max(-2,1-m)}^{2} (\mathbf{ss1}_n^{m,m'} I_{n+2}^{m+m'} + \mathbf{ss2}_n^{-m,-m'} I_{n+2}^{-(m+m')})\, Y_n^m \\
&\quad + \sum_{m=1}^{n}\sum_{m'=\max(-2,1-m)}^{2} (\mathbf{ss2}_n^{m,m'} I_{n+2}^{m+m'} + \mathbf{ss1}_n^{-m,-m'} I_{n+2}^{-(m+m')})\, Y_n^{-m} \\
&= I_{n+2}^0\left\{\mathbf{ss1}_n^{0,0} + 2\sum_{m=1}^{2}(\mathbf{ss1}_n^{m,-m}\ Y_n^m + \mathbf{ss2}_n^{m,-m}\ Y_n^{-m})\right\} \\
&\quad + \sum_{m=0}^{n}\sum_{m'=\max(-2,1-m)}^{2} (\mathbf{ss1}_n^{m,m'} I_{n+2}^{m+m'} - \mathbf{ss2}_n^{*m,m'} I_{n+2}^{-(m+m')})\, Y_n^m \\
&\quad + \sum_{m=1}^{n}\sum_{m'=\max(-2,1-m)}^{2} (\mathbf{ss2}_n^{m,m'} I_{n+2}^{m+m'} + \mathbf{ss1}_n^{*m,m'} I_{n+2}^{-(m+m')})\, Y_n^{-m}.
\end{aligned} \tag{22}$$

Table 1
Coefficient tensors $\mathbf{ss1}_n^{m,m'}$, $\mathbf{ss1}_n^{*m,m'}$, $\mathbf{ss2}_n^{m,m'}$, $\mathbf{ss2}_n^{*m,m'}$

m'	$\mathbf{ss1}_n^{m,m'}$, $\mathbf{ss1}_n^{*m,m'}$	$\mathbf{ss2}_n^{m,m'}$, $\mathbf{ss2}_n^{*m,m'}$
−2	$\frac{1}{4}(\boldsymbol{\delta}_{xx} - \boldsymbol{\delta}_{yy})$	$-\frac{1}{4}(\boldsymbol{\delta}_{xy} + \boldsymbol{\delta}_{yx})$
−1	$\frac{1}{2}(n+m+1)(\boldsymbol{\delta}_{xz} + \boldsymbol{\delta}_{zx})$	$\frac{1}{2}(n+m+1)(\boldsymbol{\delta}_{yz} + \boldsymbol{\delta}_{zy})$
0	$-\frac{1}{2}\pi_2(n+m+1)[(\boldsymbol{\delta}_{xx} + \boldsymbol{\delta}_{yy} - 2\boldsymbol{\delta}_{zz})$ $(\pm)\frac{1}{2}\delta_{m,1}(\boldsymbol{\delta}_{xx} - \boldsymbol{\delta}_{yy})]$	$-(\pm)\frac{1}{4}\delta_{m,1}\pi_2(n+2)(\boldsymbol{\delta}_{xy} + \boldsymbol{\delta}_{yx})$
1	$-\frac{1}{2}\pi_3(n+m+1)(\boldsymbol{\delta}_{xz} + \boldsymbol{\delta}_{zx})$	$\frac{1}{2}\pi_3(n+m+1)(\boldsymbol{\delta}_{yz} + \boldsymbol{\delta}_{zy})$
2	$\frac{1}{4}\pi_4(n+m+1)(\boldsymbol{\delta}_{xx} - \boldsymbol{\delta}_{yy})$	$-\frac{1}{4}\pi_4(n+m+1)(\boldsymbol{\delta}_{xy} + \boldsymbol{\delta}_{yx})$

Note that $\mathbf{ss1}_n^{m,m'} = \mathbf{ss1}_n^{*m,m'}$ and $\mathbf{ss2}_n^{m,m'} = \mathbf{ss2}_n^{*m,m'}$ except for the sign of the additional term for $m=1, m'=0$: the upper sign in $(\pm)$ applies to **ss1** and **ss2** and the lower one to $\mathbf{ss1}^*$ and $\mathbf{ss2}^*$.

The coefficients $\mathbf{ss1}_n^m$ and $\mathbf{ss2}_n^m$ are found after exceedingly tedious algebra from repeated use of Eqs. (18) and are assembled in Table 1. In Eq. (22) the factor 2 has been inserted in front of the sums for I_{n+2}^0 for convenience, because of the peculiar behavior of the **ss** for this special case. Similarly, the **ss** for negative first superscripts m have been found to be identical to their positive superscript counterparts as indicated, except for the special case of $m=0$, leading to the introduction of the $\mathbf{ss1}^*$ and $\mathbf{ss2}^*$.

Since the **ss1** and **ss2** are third rank tensors (with mostly zero elements), each of the vector elements in Table 1 are 3×3 tensors in (s_x,s_y,s_z)-space through the $\boldsymbol{\delta_{ij}}$, which are defined as 3×3 tensors with all zero elements, except the (i,j)th element, which is unity. For example,

$$\boldsymbol{\delta_{yx}}=\begin{pmatrix}0&0&0\\1&0&0\\0&0&0\end{pmatrix}. \tag{23}$$

Similar calculations may be carried out for the other three directional double operators, leading to

$$\begin{aligned}(2n+1)\nabla_{\mathrm{s}}\mathscr{L}_n J_n = I_n^0\left\{\mathbf{sl1}_n^{0,0}+2\sum_{m=1}^{2}(\mathbf{sl1}_n^{m,-m}\,Y_n^m+\mathbf{sl2}_n^{m,-m}\,Y_n^{-m})\right\}\\ +\sum_{m=0}^{n}\sum_{m'=\max(-2,1-m)}^{\min(2,n-m)}(\mathbf{sl1}_n^{m,m'}I_n^{m+m'}-\mathbf{sl2}_n^{*m,m'}I_n^{-(m+m')})\,Y_n^m\\ +\sum_{m=1}^{n}\sum_{m'=\max(-2,1-m)}^{\min(2,n-m)}(\mathbf{sl2}_n^{m,m'}I_n^{m+m'}+\mathbf{sl1}_n^{*m,m'}I_n^{-(m+m')})\,Y_n^{-m},\end{aligned} \tag{24}$$

$$\begin{aligned}(2n+1)\mathscr{L}_{n-1}\nabla_{\mathrm{s}}J_n = I_n^0\left\{\mathbf{ls1}_n^{0,0}+2\sum_{m=1}^{2}(\mathbf{ls1}_n^{m,-m}\,Y_n^m+\mathbf{ls2}_n^{m,-m}\,Y_n^{-m})\right\}\\ +\sum_{m=0}^{n}\sum_{m'=\max(-2,1-m)}^{\min(2,n-m)}(\mathbf{ls1}_n^{m,m'}I_n^{m+m'}-\mathbf{ls2}_n^{*m,m'}I_n^{-(m+m')})\,Y_n^m\\ +\sum_{m=1}^{n}\sum_{m'=\max(-2,1-m)}^{\min(2,n-m)}(\mathbf{ls2}_n^{m,m'}I_n^{m+m'}+\mathbf{ls1}_n^{*m,m'}I_n^{-(m+m')})\,Y_n^{-m},\end{aligned} \tag{25}$$

$$\begin{aligned}(2n-3)\mathscr{L}_{n-1}\mathscr{L}_{n-2}J_{n-2} = I_{n-2}^0\left\{\mathbf{ll1}_n^{0,0}+2\sum_{m=1}^{2}(\mathbf{ll1}_n^{m,-m}\,Y_n^m+\mathbf{ll2}_n^{m,-m}\,Y_n^{-m})\right\}\\ +\sum_{m=0}^{n}\sum_{m'=\max(-2,1-m)}^{\min(2,n-m-2)}(\mathbf{ll1}_n^{m,m'}I_{n-2}^{m+m'}-\mathbf{ll2}_n^{*m,m'}I_{n-2}^{-(m+m')})\,Y_n^m\\ +\sum_{m=1}^{n}\sum_{m'=\max(-2,1-m)}^{\min(2,n-m)}(\mathbf{ll2}_n^{m,m'}I_{n-2}^{m+m'}+\mathbf{ll1}_n^{*m,m'}I_{n-2}^{-(m+m')})\,Y_n^{-m},\end{aligned} \tag{26}$$

with coefficient tensors $\mathbf{sl1}_n^m$ and $\mathbf{sl2}_n^m$ assembled in Table 2, $\mathbf{ls1}_n^m$ and $\mathbf{ls2}_n^m$ in Table 3, and $\mathbf{ll1}_n^{m,m'}$ and $\mathbf{ll2}_n^{m,m'}$ in Table 4.

Table 2
Coefficient tensors $\mathbf{sl1}_n^{m,m'}$, $\mathbf{sl1}_n^{*m,m'}$, $\mathbf{sl2}_n^{m,m'}$, $\mathbf{sl2}_n^{*m,m'}$

m'	$\mathbf{sl1}_n^{m,m'}$, $\mathbf{sl1}_n^{*m,m'}$	$\mathbf{sl2}_n^{m,m'}$, $\mathbf{sl2}_n^{*m,m'}$
-2	$-\frac{1}{4}(\boldsymbol{\delta}_{xx}-\boldsymbol{\delta}_{yy})$	$\frac{1}{4}(\boldsymbol{\delta}_{xy}+\boldsymbol{\delta}_{yx})$
-1	$\frac{1}{2}[(n-m+2)\boldsymbol{\delta}_{xz}-(n+m+1)\boldsymbol{\delta}_{zx}]$	$\frac{1}{2}[(n-m+2)\boldsymbol{\delta}_{yz}-(n+m+1)\boldsymbol{\delta}_{zy}]$
0	$\frac{1}{4}[\pi_2(n+m+1)+\pi_2(n-m+1)](\boldsymbol{\delta}_{xx}+\boldsymbol{\delta}_{yy})$ $+(n+m+1)(n-m+1)\boldsymbol{\delta}_{zz}(\pm)\frac{1}{4}\delta_{m,1}\pi_2(n)(\boldsymbol{\delta}_{xx}-\boldsymbol{\delta}_{yy})$	$\frac{1}{4}[\pi_2(n+m+1)-\pi_2(n-m+1)](\boldsymbol{\delta}_{xy}-\boldsymbol{\delta}_{yx})$ $(\pm)\frac{1}{4}\delta_{m,1}\pi_2(n)(\boldsymbol{\delta}_{xy}+\boldsymbol{\delta}_{yx})$
1	$-\frac{1}{2}(n+m+1)(n-m)[(n+m+2)\boldsymbol{\delta}_{xz}-(n-m+1)\boldsymbol{\delta}_{zx}]$	$\frac{1}{2}(n+m+1)(n-m)[(n+m+2)\boldsymbol{\delta}_{yz}-(n-m+1)\boldsymbol{\delta}_{zy}]$
2	$-\frac{1}{4}\pi_2(n+m+1)\pi_2(n-m-1)(\boldsymbol{\delta}_{xx}-\boldsymbol{\delta}_{yy})$	$\frac{1}{4}\pi_2(n+m+1)\pi_2(n-m-1)(\boldsymbol{\delta}_{xy}+\boldsymbol{\delta}_{yx})$

Note that $\mathbf{sl1}_n^{m,m'}=\mathbf{sl1}_n^{*m,m'}$ and $\mathbf{sl2}_n^{m,m'}=\mathbf{sl2}_n^{*m,m'}$ except for the sign of the additional term for $m=1,m'=0$: the upper sign in $(\pm)$ applies to **sl1** and **sl2** and the lower one to $\mathbf{sl1}^*$ and $\mathbf{sl2}^*$.

Table 3
Coefficients tensors $\mathbf{ls1}_n^{m,m'}$, $\mathbf{ls1}_n^{*m,m'}$, $\mathbf{ls2}_n^{m,m'}$, $\mathbf{ls2}_n^{*m,m'}$

m'	$\mathbf{ls1}_n^{m,m'}$, $\mathbf{ls1}_n^{*m,m'}$	$\mathbf{ls2}_n^{m,m'}$, $\mathbf{ls2}_n^{*m,m'}$
-2	$-\frac{1}{4}(\boldsymbol{\delta}_{xx}-\boldsymbol{\delta}_{yy})$	$\frac{1}{4}(\boldsymbol{\delta}_{xy}+\boldsymbol{\delta}_{yx})$
-1	$-\frac{1}{2}(n+m-1)\boldsymbol{\delta}_{xz}+\frac{1}{2}(n-m)\boldsymbol{\delta}_{zx}$	$-\frac{1}{2}(n+m-1)\boldsymbol{\delta}_{yz}+\frac{1}{2}(n-m)\boldsymbol{\delta}_{zy}$
0	$\frac{1}{4}[\pi_2(n+m-1)+\pi_2(n-m-1)](\boldsymbol{\delta}_{xx}+\boldsymbol{\delta}_{yy})$ $+(n+m)(n-m)\boldsymbol{\delta}_{zz}(\pm)\frac{1}{4}\delta_{m,1}\pi_2(n)(\boldsymbol{\delta}_{xx}-\boldsymbol{\delta}_{yy})$	$\frac{1}{4}[\pi_2(n-m-1)-\pi_2(n+m-1)](\boldsymbol{\delta}_{xy}-\boldsymbol{\delta}_{yx})$ $(\pm)\frac{1}{4}\delta_{m,1}\pi_2(n)(\boldsymbol{\delta}_{xy}+\boldsymbol{\delta}_{yx})$
1	$\frac{1}{2}(n+m+1)(n-m)[(n-m-1)\boldsymbol{\delta}_{xz}-(n+m)\boldsymbol{\delta}_{zx}]$	$-\frac{1}{2}(n+m+1)(n-m)[(n-m-1)\boldsymbol{\delta}_{yz}-(n+m)\boldsymbol{\delta}_{zy}]$
2	$-\frac{1}{4}\pi_2(n+m+1)\pi_2(n-m-1)(\boldsymbol{\delta}_{xx}-\boldsymbol{\delta}_{yy})$	$\frac{1}{4}\pi_2(n+m+1)\pi_2(n-m-1)(\boldsymbol{\delta}_{xy}+\boldsymbol{\delta}_{yx})$

Note that $\mathbf{ls1}_n^{m,m'}=\mathbf{ls1}_n^{*m,m'}$ and $\mathbf{ls2}_n^{m,m'}=\mathbf{ls2}_n^{*m,m'}$ except for the sign of the additional term for $m=1,m'=0$: the upper sign in $(\pm)$ applies to **ls1** and **ls2** and the lower one to $\mathbf{ls1}^*$ and $\mathbf{ls2}^*$.

Table 4
Coefficient tensors $\mathbf{ll1}_n^{m,m'}$, $\mathbf{ll1}_n^{*m,m'}$, $\mathbf{ll2}_n^{m,m'}$, $\mathbf{ll2}_n^{*m,m'}$

m'	$\mathbf{ll1}_n^{m,m'}$, $\mathbf{ll1}_n^{*m,m'}$	$\mathbf{ll2}_n^{m,m'}$, $\mathbf{ll2}_n^{*m,m'}$
-2	$\frac{1}{4}(\boldsymbol{\delta}_{xx}-\boldsymbol{\delta}_{yy})$	$-\frac{1}{4}(\boldsymbol{\delta}_{xy}+\boldsymbol{\delta}_{yx})$
-1	$-\frac{1}{2}(n-m)(\boldsymbol{\delta}_{xz}+\boldsymbol{\delta}_{zx})$	$-\frac{1}{2}(n-m)(\boldsymbol{\delta}_{yz}+\boldsymbol{\delta}_{zy})$
0	$-\frac{1}{2}\pi_2(n-m-1)[(\boldsymbol{\delta}_{xx}+\boldsymbol{\delta}_{yy}-2\boldsymbol{\delta}_{zz})$ $(\pm)\frac{1}{2}\delta_{m,1}(\boldsymbol{\delta}_{xx}-\boldsymbol{\delta}_{yy})]$	$-(\pm)\frac{1}{4}\pi_2(n-2)\delta_{m,1}(\boldsymbol{\delta}_{xy}+\boldsymbol{\delta}_{yx})$
1	$\frac{1}{2}\pi_3(n-m-2)(\boldsymbol{\delta}_{xz}+\boldsymbol{\delta}_{zx})$	$-\frac{1}{2}\pi_3(n-m-2)(\boldsymbol{\delta}_{yz}+\boldsymbol{\delta}_{zy})$
2	$\frac{1}{4}\pi_4(n-m-3)(\boldsymbol{\delta}_{xx}-\boldsymbol{\delta}_{yy})$	$-\frac{1}{4}\pi_4(n-m-3)(\boldsymbol{\delta}_{xy}+\boldsymbol{\delta}_{yx})$

Note that $\mathbf{ll1}_n^{m,m'}=\mathbf{ll1}_n^{*m,m'}$ and $\mathbf{ll2}_n^{m,m'}=\mathbf{ll2}_n^{*m,m'}$ except for the sign of the additional term for $m=1,m'=0$: the upper sign in $(\pm)$ applies to **ll1** and **ll2** and the lower one to $\mathbf{ll1}^*$ and $\mathbf{ll2}^*$.

Sticking Eqs. (22), (24)–(26) into Eq. (16) and collecting coefficients of the Y_n^m harmonic yields $2n+1$ independent, elliptic partial differential equations:

$Y_n^m, 0 \leqslant m \leqslant n$:

$$\begin{aligned}
&\frac{1}{2n+5}\left[\nabla_\tau\left(\frac{1}{\alpha_{n+1}}\nabla_\tau\right)\right]^{\mathrm{T}}:\left\{(2-\delta_{m,0})\mathbf{ss1}_n^{m,-m}I_{n+2}^0+\sum_{m'=\max(-2,1-m)}^{2}(\mathbf{ss1}_n^{m,m'}I_{n+2}^{m+m'}-\mathbf{ss2}_n^{*m,m'}I_{n+2}^{-(m+m')})\right\}\\
&+\frac{1}{2n+1}\left[\nabla_\tau\left(\frac{1}{\alpha_{n+1}}\nabla_\tau\right)\right]^{\mathrm{T}}:\left\{(2-\delta_{m,0})\mathbf{sl1}_n^{m,-m}I_n^0+\sum_{m'=\max(-2,1-m)}^{\min(2,n-m)}(\mathbf{sl1}_n^{m,m'}I_n^{m+m'}-\mathbf{sl2}_n^{*m,m'}I_n^{-(m+m')})\right\}\\
&+\frac{1}{2n+1}\left[\nabla_\tau\left(\frac{1}{\alpha_{n-1}}\nabla_\tau\right)\right]^{\mathrm{T}}:\left\{(2-\delta_{m,0})\mathbf{ls1}_n^{m,-m}I_n^0+\sum_{m'=\max(-2,1-m)}^{\min(2,n-m)}(\mathbf{ls1}_n^{m,m'}I_n^{m+m'}-\mathbf{ls2}_n^{*m,m'}I_n^{-(m+m')})\right\}\\
&+\frac{1}{2n-3}\left[\nabla_\tau\left(\frac{1}{\alpha_{n-1}}\nabla_\tau\right)\right]^{\mathrm{T}}:\left\{(2-\delta_{m,0})\mathbf{ll1}_n^{m,-m}I_{n-2}^0+\sum_{m'=\max(-2,1-m)}^{\min(2,n-m-2)}(\mathbf{ll1}_n^{m,m'}I_{n-2}^{m+m'}-\mathbf{ll2}_n^{*m,m'}I_n^{-(m+m')})\right\}\\
&-\frac{\alpha_n}{2n+1}\left(I_n^m-4\pi I_{\mathrm{b}}\delta_{n,0}\delta_{m,0}\right)=0, \qquad (27a)
\end{aligned}$$

$Y_n^{-m}, 1 \leqslant m \leqslant n$:

$$\begin{aligned}
&\frac{1}{2n+5}\left[\nabla_\tau\left(\frac{1}{\alpha_{n+1}}\nabla_\tau\right)\right]^{\mathrm{T}}:\left\{2\mathbf{ss2}_n^{m,-m}I_{n+2}^0+\sum_{m'=\max(-2,1-m)}^{2}(\mathbf{ss2}_n^{m,m'}I_{n+2}^{m+m'}+\mathbf{ss1}_n^{*m,m'}I_{n+2}^{-(m+m')})\right\}\\
&+\frac{1}{2n+1}\left[\nabla_\tau\left(\frac{1}{\alpha_{n+1}}\nabla_\tau\right)\right]^{\mathrm{T}}:\left\{2\mathbf{sl2}_n^{m,-m}I_n^0+\sum_{m'=\max(-2,1-m)}^{\min(2,n-m)}(\mathbf{sl2}_n^{m,m'}I_n^{m+m'}+\mathbf{sl1}_n^{*m,m'}I_n^{-(m+m')})\right\}\\
&+\frac{1}{2n+1}\left[\nabla_\tau\left(\frac{1}{\alpha_{n-1}}\nabla_\tau\right)\right]^{\mathrm{T}}:\left\{2\mathbf{ls2}_n^{m,-m}I_n^0+\sum_{m'=\max(-2,1-m)}^{\min(2,n-m)}(\mathbf{ls2}_n^{m,m'}I_n^{m+m'}+\mathbf{ls1}_n^{*m,m'}I_n^{-(m+m')})\right\}\\
&+\frac{1}{2n-3}\left[\nabla_\tau\left(\frac{1}{\alpha_{n-1}}\nabla_\tau\right)\right]^{\mathrm{T}}:\left\{2\mathbf{ll2}_n^{m,-m}I_{n-2}^0+\sum_{m'=\max(-2,1-m)}^{\min(2,n-m-2)}(\mathbf{ll2}_n^{m,m'}I_{n-2}^{m+m'}+\mathbf{ll1}_n^{*m,m'}I_n^{-(m+m')})\right\}\\
&-\frac{\alpha_n}{2n+1}I_n^{-m}=0. \qquad (27b)
\end{aligned}$$

2.3. Sample results of RTE transformation

As an example we will extract the P_3 approximation from Eq. (27). Applying these equations for $n=0$ and 2 yields

Y_n^0, $n=0$:

$$\begin{aligned}
&\frac{1}{5}\left[\nabla_\tau\left(\frac{1}{\alpha_1}\nabla_\tau\right)\right]^{\mathrm{T}}:\left\{\mathbf{ss1}_0^{0,0}I_2^0+\mathbf{ss1}_0^{0,1}I_2^1-\mathbf{ss2}_0^{*0,1}I_2^{-1}+\mathbf{ss1}_0^{0,2}I_2^2-\mathbf{ss2}_0^{*0,2}I_2^{-2}\right\}\\
&+\left[\nabla_\tau\left(\frac{1}{\alpha_1}\nabla_\tau\right)\right]^{\mathrm{T}}:\left\{\mathbf{sl1}_0^{0,0}I_0\right\}-\alpha_0(I_0-4\pi I_{\mathrm{b}})=0, \qquad (28)
\end{aligned}$$

Y_n^0, $n=2$, $m=0$:

$$\frac{1}{5}\left[\nabla_\tau\left(\frac{1}{\alpha_3}\nabla_\tau\right)\right]^{\mathrm{T}}:\left\{\mathbf{sl1}_2^{0,0}I_2^0+\mathbf{sl1}_2^{0,1}I_2^1-\mathbf{sl2}_2^{*0,1}I_2^{-1}+\mathbf{sl1}_2^{0,2}I_2^2-\mathbf{sl2}_2^{*0,2}I_2^{-2}\right\}$$

$$+\frac{1}{5}\left[\nabla_\tau\left(\frac{1}{\alpha_1}\nabla_\tau\right)\right]^{\mathrm{T}}:\left\{\mathbf{ls1}_2^{0,0}I_2^0+\mathbf{ls1}_2^{0,1}I_2^1-\mathbf{ls2}_2^{*0,1}I_2^{-1}+\mathbf{ls1}_2^{0,2}I_2^2-\mathbf{ls2}_2^{*0,2}I_2^{-2}\right\}$$
$$+\left[\nabla_\tau\left(\frac{1}{\alpha_1}\nabla_\tau\right)\right]^{\mathrm{T}}:\{\mathbf{ll1}_2^{0,0}I_0\}-\frac{\alpha_2}{5}I_2^0=0, \tag{29}$$

Y_n^m, $n=2$, $m=1,2$:

$$\frac{1}{5}\left[\nabla_\tau\left(\frac{1}{\alpha_3}\nabla_\tau\right)\right]^{\mathrm{T}}:\{2\mathbf{sl1}_2^{m,-m}I_2^0+\mathbf{sl1}_2^{m,1-m}I_2^1-\mathbf{sl2}_2^{*m,1-m}I_2^{-1}+\mathbf{sl1}_2^{m,2-m}I_2^2-\mathbf{sl2}_2^{*m,2-m}I_2^{-2}\}$$
$$+\frac{1}{5}\left[\nabla_\tau\left(\frac{1}{\alpha_1}\nabla_\tau\right)\right]^{\mathrm{T}}:\{2\mathbf{ls1}_2^{m,-m}I_2^0+\mathbf{ls1}_2^{m,1-m}I_2^1-\mathbf{ls2}_2^{*m,1-m}I_2^{-1}+\mathbf{ls1}_2^{m,2-m}I_2^2-\mathbf{ls2}_2^{*m,2-m}I_2^{-2}\}$$
$$+\left[\nabla_\tau\left(\frac{1}{\alpha_1}\nabla_\tau\right)\right]^{\mathrm{T}}:\{2\mathbf{ll1}_2^{m,-m}I_0\}-\frac{\alpha_2}{5}I_2^m=0, \tag{30}$$

Y_n^{-m}, $n=2$, $m=1,2$:

$$\frac{1}{5}\left[\nabla_\tau\left(\frac{1}{\alpha_3}\nabla_\tau\right)\right]^{\mathrm{T}}:\left\{2\mathbf{sl2}_2^{m,-m}I_2^0+\mathbf{sl2}_2^{m,1-m}I_2^1+\mathbf{sl1}_2^{*m,1-m}I_2^{-1}+\mathbf{sl2}_2^{m,2-m}I_2^2+\mathbf{sl1}_2^{*m,2-m}I_2^{-2}\right\}$$

$$+\frac{1}{5}\left[\nabla_\tau\left(\frac{1}{\alpha_1}\nabla_\tau\right)\right]^{\mathrm{T}}:\{2\mathbf{ls2}_2^{m,-m}I_2^0+\mathbf{ls2}_2^{m,1-m}I_2^1+\mathbf{ls1}_2^{*m,1-m}I_2^{-1}+\mathbf{ls2}_2^{m,2-m}I_2^2+\mathbf{ls1}_2^{*m,2-m}I_2^{-2}\}$$
$$+\left[\nabla_\tau\left(\frac{1}{\alpha_1}\nabla_\tau\right)\right]^{\mathrm{T}}:\{2\mathbf{ll2}_2^{m,-m}I_0\}-\frac{\alpha_2}{5}I_2^{-m}=0. \tag{31}$$

Note that in Eq. (28) the third and fourth operator terms do not appear: I_{n-2}^m does not exist and the $\mathscr{L}_{n-1}\nabla_{\mathrm{s}}$ operator first transforms Y_n^m to Y_{n-1}^m (which does not exist) through use of ∇_{s}, before the $\mathscr{L}_{n-1}$ operator brings it back to level n. In the $n=2$ equations the first operator term does not appear, since I_4^m is presumed to be zero.

Here we will limit our study to a two-dimensional enclosure without dependence in the z-direction (as shown in Fig. 1). Due to the symmetry of the intensity field about the x-y-plane, which requires

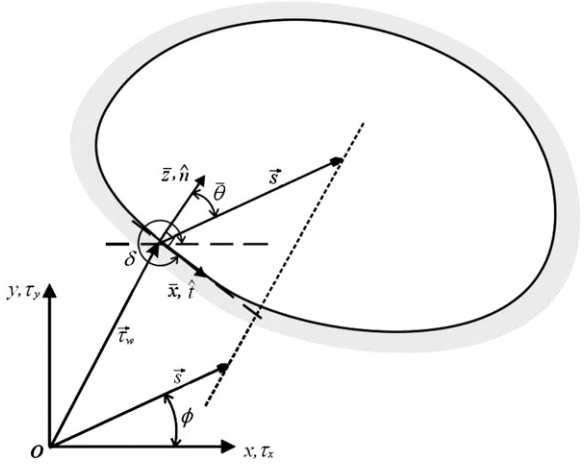

Fig. 1. Local and global coordinates for a two-dimensional enclosure.

$I(\theta,\phi)=I(\pi-\theta,\phi)$, the coefficients associated with spherical harmonics Y_2^{-1} and Y_2^1 are then shown to be zero (as well as I_1^0, I_3^{-2}, I_3^0 and I_3^2, i.e., all with $n+m$ odd). Thus, the six PDEs from Eqs. (28) through (31) reduce to four coupled elliptic PDEs as summarized below:

$$\frac{\partial}{\partial\tau_x}\left[2\gamma_{8,3}\frac{\partial I_2^{-2}}{\partial\tau_x}-\gamma_{1,1}\frac{\partial I_2^0}{\partial\tau_y}+2\gamma_{7,-3}\frac{\partial I_2^2}{\partial\tau_y}+\frac{5}{\alpha_1}\frac{\partial I_0}{\partial\tau_y}\right]+\frac{\partial}{\partial\tau_y}\left[2\gamma_{8,3}\frac{\partial I_2^{-2}}{\partial\tau_y}-\gamma_{1,1}\frac{\partial I_2^0}{\partial\tau_x}-2\gamma_{7,-3}\frac{\partial I_2^2}{\partial\tau_x}+\frac{5}{\alpha_1}\frac{\partial I_0}{\partial\tau_x}\right]-2\alpha_2 I_2^{-2}=0\quad\text{for } Y_2^{-2}, \tag{32a}$$

$$\frac{\partial}{\partial\tau_x}\left[\gamma_{6,1}\frac{\partial I_2^0}{\partial\tau_x}-6\gamma_{1,1}\frac{\partial I_2^2}{\partial\tau_x}-6\gamma_{1,1}\frac{\partial I_2^{-2}}{\partial\tau_y}-\frac{5}{\alpha_1}\frac{\partial I_0}{\partial\tau_x}\right]+\frac{\partial}{\partial\tau_y}\left[\gamma_{6,1}\frac{\partial I_2^0}{\partial\tau_y}+6\gamma_{1,1}\frac{\partial I_2^2}{\partial\tau_y}-6\gamma_{1,1}\frac{\partial I_2^{-2}}{\partial\tau_x}-\frac{5}{\alpha_1}\frac{\partial I_0}{\partial\tau_y}\right]-\alpha_2 I_2^0=0\quad\text{for } Y_2^0, \tag{32b}$$

$$\frac{\partial}{\partial\tau_x}\left[2\gamma_{8,3}\frac{\partial I_2^2}{\partial\tau_x}-\gamma_{1,1}\frac{\partial I_2^0}{\partial\tau_x}-2\gamma_{7,-3}\frac{\partial I_2^{-2}}{\partial\tau_y}+\frac{5}{\alpha_1}\frac{\partial I_0}{\partial\tau_x}\right]+\frac{\partial}{\partial\tau_y}\left[2\gamma_{8,3}\frac{\partial I_2^2}{\partial\tau_y}+\gamma_{1,1}\frac{\partial I_2^0}{\partial\tau_y}+2\gamma_{7,-3}\frac{\partial I_2^{-2}}{\partial\tau_x}-\frac{5}{\alpha_1}\frac{\partial I_0}{\partial\tau_y}\right]-2\alpha_2 I_2^2=0\quad\text{for } Y_2^2, \tag{32c}$$

$$\frac{\partial}{\partial\tau_x}\left[\frac{5}{\alpha_1}\frac{\partial I_0}{\partial\tau_x}-\frac{1}{\alpha_1}\frac{\partial I_2^0}{\partial\tau_x}+\frac{6}{\alpha_1}\frac{\partial I_2^2}{\partial\tau_x}+\frac{6}{\alpha_1}\frac{\partial I_2^{-2}}{\partial\tau_y}\right]+\frac{\partial}{\partial\tau_y}\left[\frac{5}{\alpha_1}\frac{\partial I_0}{\partial\tau_y}-\frac{1}{\alpha_1}\frac{\partial I_2^0}{\partial\tau_y}-\frac{6}{\alpha_1}\frac{\partial I_2^2}{\partial\tau_y}+\frac{6}{\alpha_1}\frac{\partial I_2^{-2}}{\partial\tau_x}\right]=5\alpha_0(I_0-4\pi I_b)\quad\text{for } Y_0, \tag{32d}$$

where

$$\gamma_{i,j}=\left(\frac{i}{\alpha_3}+\frac{j}{\alpha_1}\right). \tag{33}$$

2.4. Boundary conditions and supplementary conditions

Since intensity is expressed as a truncated series of spherical harmonics, Eqs. (1)–(3), boundary conditions can only be satisfied approximately. This is done by minimizing the difference between $I(\vec{\tau}=\vec{\tau}_w,\hat{s})$ (as predicted by the P_N approximation) and the actual surface intensity $I_s(\vec{\tau}_w,\hat{s})$ over the hemisphere covering all outgoing directions, $\hat{n}\cdot\hat{s}>0$, everywhere on the surface, as described by vector $\vec{\tau}_w$ and shown in Fig. 1. There are several minimization schemes, the most popular ones proposed by Mark [16,17] and by Marshak [18]. For more general problems, Marshak's boundary condition appears to be more flexible and accurate since it minimizes the difference in an integral sense. Here, Marshak's boundary conditions are used together with the supplementary conditions of Eq. (14). The general form of Marshak's boundary condition can be summarized as

$$\int_{\hat{n}\cdot\hat{s}>0} I(\tau_w,\hat{s})\,\bar{Y}_{2i-1}^m\,d\Omega=\int_{\hat{n}\cdot\hat{s}>0} I_s(\tau_w,\hat{s})\,\bar{Y}_{2i-1}^m\,d\Omega,\quad i=1,2,\ldots,\frac{1}{2}(N+1),\ \text{all relevant } m, \tag{34}$$

where $\bar{Y}$ denotes spherical harmonics measured from a local spherical coordinate system, with polar angle $\bar{\theta}$ measured from the surface normal (local $\bar{z}$-axis), and $\bar{\phi}$ in the plane of the surface (measured from a local $\bar{x}$-axis). "All relevant m" implies choosing a set consistent with the P_N-approximation. For example, for the P_3 approximation six boundary conditions are needed: $i=1$ provides three ($m=-1,0,+1$), and another three must come from $i=2$ (usually chosen as the smallest m-values, i.e., $m=-1,0,+1$).

In general, of course, the local surface normal does not coincide with the global z-axis. Thus, in order to obtain a generic boundary condition for arbitrary geometries, the global spherical harmonics must be rotated into the local coordinate system for the evaluation of Eq. (34). Such rotation, according to Euler's rotation

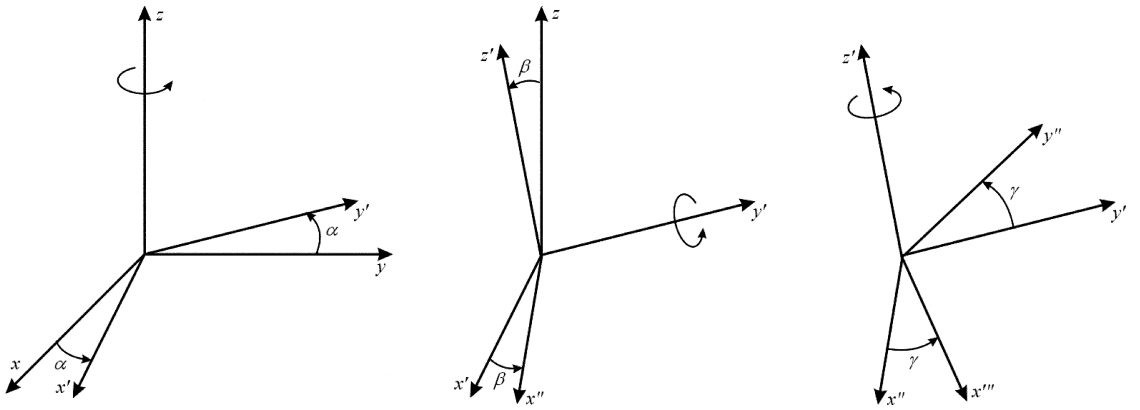

Fig. 2. Definition of Euler angles for an arbitrary rotation.

theorem, may be described using three angles, which are called Euler angles. In the literature, there are several notation and rotation conventions for Euler angles. Here, the notation (α, β, γ) is used for three Euler angles following Varshalovich's definition [19]. In Varshalovich's convention, as shown in Fig. 2, an arbitrary rotation is defined by Euler angles (α, β, γ), where the first rotation is by an angle α about the z-axis, the second is by an angle β about the y'-axis, and the third is by an angle γ about the z'-axis. As indicated in Fig. 2 all three rotations are, following the right-hand-rule, in counter-clockwise direction about the center axis. The three rotations can, in general, be carried out by (1) rotating x–y so that y' is perpendicular to $\hat{n}$ ($\hat{n} \cdot \hat{y}' = 0$):

$$\hat{i}' = \cos\alpha\hat{i} + \sin\alpha\hat{j}; \quad \hat{j}' = -\sin\alpha\hat{i} + \cos\alpha\hat{j} \tag{35}$$

and

$$\tan\alpha = \frac{n_y}{n_x}, \tag{36}$$

(2) rotating $x'-z$ such that z' becomes parallel to $\hat{n}$, or

$$\hat{k}' = \sin\beta\hat{i}' + \cos\beta\hat{k} \tag{37}$$

and $\hat{n} \cdot \hat{k}' = 1$ gives

$$(n_x \cos\alpha + n_y \sin\alpha)\sin\beta + n_z \cos\beta = 1. \tag{38}$$

(3) The third rotation is arbitrary and serves to place the local $\bar{x}-\bar{y}$-coordinates into convenient locations. For example, to perform the transformation indicated in Fig. 1 (with the global z-axis pointing toward the reader), the local surface normal is determined as

$$\hat{n} = -\sin\delta\hat{i} + \cos\delta\hat{j} + 0\hat{k}, \tag{39}$$

and the first rotation angle α follows from

$$\tan\alpha = -\tan\delta \quad \text{or } \alpha = \delta \pm \frac{\pi}{2}. \tag{40}$$

If we choose $\alpha = \delta - \pi/2$ (y' points into the indicated $\bar{x}$-direction), the second rotation angle becomes

$$\left[-\sin\delta\cos\left(\delta - \frac{\pi}{2}\right) + \cos\delta\sin\left(\delta - \frac{\pi}{2}\right)\right]\sin\beta = 1 \quad \text{or } \beta = \frac{3\pi}{2}. \tag{41}$$

This has x'' point out of the paper, and a final (optional) rotation of $\gamma = \pi/2$ rotates x''' into the desired local $\bar{x}$-direction.

It can be shown that, for a given rotation, the spherical harmonics of order n are transformed into a linear combination of spherical harmonics of the same order n. Such operation can be represented in the form of a

rotation matrix, where each element of this matrix is a function of Euler angles:

$$Y_n^{m'}(\theta,\phi)=\sum_{m=-n}^{n}\Delta_{mm'}^n(\alpha,\beta,\gamma)\,\bar{Y}_n^m(\bar{\theta},\bar{\phi}), \tag{42}$$

where $\Delta_{mm'}^n(\alpha,\beta,\gamma)$ is the representation matrix of the rotation operation for the real spherical harmonics Y_n^m of order n. Blanco et al. [20] developed a closed-form expression to specify all the elements based on Wigner-D functions. However, in Blanco's derivation, a normalization factor is employed. In order to be consistent with the real spherical harmonics used in the current study, a modification coefficient $C_{mm'}^n$ for a given real spherical harmonic Y_n^m, needs to be included in the transformation:

$$C_{mm'}^n=\frac{2(-1)^{m+m'}}{1+\delta_{m,0}}\sqrt{\frac{(n-|m|)!(n+|m'|)!}{(n+|m|)!(n-|m'|)!}}, \tag{43}$$

where $\delta_{m',0}$ is Kronecker's delta. Knowing the Euler angles, the Δ^n matrices can be obtained via the relationships developed by Blanco et al. [20]:

$$\begin{aligned}\Delta_{mm'}^n &= \tfrac{1}{2}C_{mm'}^n\{\mathrm{sign}(m')\Psi_m(\alpha)\Psi_{m'}(\gamma)[d_{|m'|,|m|}^n(\beta)+(-1)^m d_{|m|,-|m'|}^n(\beta)]\\ &\quad-\mathrm{sign}(m)\Psi_{-m}(\alpha)\Psi_{-m'}(\gamma)[d_{|m'|,|m|}^n(\beta)-(-1)^m d_{|m|,-|m'|}^n(\beta)]\}\\ &=\mathrm{sign}(m')\Psi_m(\alpha)\Psi_{m'}(\gamma)[\bar{d}_{|m|,|m'|}^n(\beta)+(-1)^{m'}\bar{d}_{|m|,-|m'|}^n(\beta)]\\ &\quad-\mathrm{sign}(m)\Psi_{-m}(\alpha)\Psi_{-m'}(\gamma)[\bar{d}_{|m|,|m'|}^n(\beta)-(-1)^{m'}d_{|m|,-|m'|}^n(\beta)],\end{aligned} \tag{44}$$

where $\mathrm{sign}(0)=1$ and the function Ψ_m is defined as

$$\Psi_m(\xi)=\begin{cases}\cos m\xi & \text{for } m>0,\\ 1 & \text{for } m=0,\\ \sin|m|\xi & \text{for } m<0.\end{cases} \tag{45}$$

To determine the Δ^n matrices by Eq. (44) the $\bar{d}^n$ matrices are needed, which are modified versions of the real parts of the Wigner-$D_{mm'}^n$ functions, depending only on Euler angle β as

$$D_{mm'}^n(\alpha,\beta,\gamma)=\mathrm{e}^{-\mathrm{i}m\alpha}d_{mm'}^n(\beta)\mathrm{e}^{-\mathrm{i}m'\gamma}. \tag{46}$$

The d^n matrix has been given in closed form by Blanco et al. [19], and the modified $\bar{d}^n$ may be calculated from

$$\begin{aligned}\bar{d}_{mm'}^n(\beta) &= \frac{1}{1+\delta_{m,0}}\sqrt{\frac{(n-|m|)!(n+|m'|)!}{(n+|m|)!(n-|m'|)!}}\,d_{mm'}^n\\ &=\frac{(-1)^{m+m'}(n-|m|)!(n+|m'|)!}{1+\delta_{m,0}}\sum_{k=\max(0,m'-m)}^{\min(n-m,n+m')}\frac{(-1)^k\left(\cos\frac{\beta}{2}\right)^{2n-2k-m+m'}\left(\sin\frac{\beta}{2}\right)^{2k+m-m'}}{k!(n-m-k)!(n+m'-k)!(m-m'+k)!}.\end{aligned} \tag{47}$$

With the rotation of spherical harmonics between local and global coordinates as indicated by Eq. (42), relationships between I_n^m and $\bar{I}_n^m$ can be revealed accordingly by expressing intensity in terms of both local and global coordinates,

$$I(\tau,\hat{s})=\frac{1}{4\pi}\sum_{n}^{N}\sum_{m=-n}^{n}I_n^m(\tau)\,Y_n^m(\hat{s})=\frac{1}{4\pi}\sum_{n}^{N}\sum_{m=-n}^{n}\bar{I}_n^m(\tau)\,\bar{Y}_n^m(\hat{s}), \tag{48}$$

which leads to

$$I_n^m=\sum_{m'=-n}^{n}\Delta_{mm'}^n(\alpha,\beta,\gamma)\bar{I}_n^{m'}\quad\text{and}\quad\bar{I}_n^m=\sum_{m'=-n}^{n}\bar{\Delta}_{mm'}^n(-\gamma,-\beta,-\alpha)I_n^{m'}, \tag{49}$$

where the bar on the $\bar{\Delta}^n_{mm'}$ implies backward rotation from local to global coordinates, as indicated by the arguments. Substitution of Eq. (48) into (34) reduces the boundary conditions to

$$\sum_{n=0}^{N}\left[\int_0^1 P_n^m(\bar{\mu})P_{2i-1}^m(\bar{\mu})\,\mathrm{d}\bar{\mu}\right]\bar{I}_n^m(\tau_w)=\frac{4}{1+\delta_{m,0}}\int_0^{2\pi}\int_0^1 I_s(\bar{\mu}=\cos\bar{\theta},\bar{\psi})\,\bar{Y}_{2i-1}^m(\bar{\mu},\bar{\psi})\,\mathrm{d}\bar{\mu}\,\mathrm{d}\bar{\psi},$$
$$i=1,2,\ldots,\frac{1}{2}(N+1),\ \text{ all relevant } m. \tag{50}$$

If the surface intensity I_s is diffuse, this simplifies to

$$\sum_{n=0}^{N}\left[\int_0^1 P_n^m(\bar{\mu})P_{2i-1}^m(\bar{\mu})\,\mathrm{d}\bar{\mu}\right]\bar{I}_n^m(\tau_w)=\left[\int_0^1 P_{2i-1}(\bar{\mu})\,\mathrm{d}\bar{\mu}\right]\delta_{m,0}\,4\pi I_s,$$
$$i=1,2,\ldots,\frac{1}{2}(N+1),\ \text{ all relevant } m, \tag{51}$$

or

$$\sum_{n=0}^{N}p_{n,2i-1}^m\bar{I}_n^m=4\pi I_s p_{0,2i-1}^0\delta_{m,0}, \tag{52}$$

with $p_{n,j}^m$ defined as

$$p_{n,j}^m=p_{j,n}^m=\int_0^1 P_n^m(\bar{\mu})P_j^m(\bar{\mu})\,\mathrm{d}\bar{\mu}. \tag{53}$$

Before these boundary conditions can be applied to Eqs. (27) the $\bar{I}_n^m$ with odd n must be eliminated using the compatibility condition (14), and local coefficient functions $\bar{I}_n^m$ must be converted to global I_n^m, Eq. (49). Applying the operators of Eqs. (18) and (20) to Eq. (14) leads to

$$\frac{\bar{I}_n^0}{2n+1}=\frac{1}{2\alpha_n}\frac{\partial}{\partial\tau_{\bar{x}}}\left[\frac{\pi_2(n+1)}{2n+3}\bar{I}_{n+1}^1-\frac{\pi_2(n-1)}{2n-1}\bar{I}_{n-1}^1\right]+\frac{1}{2\alpha_n}\frac{\partial}{\partial\tau_{\bar{y}}}\left[\frac{\pi_2(n+1)}{2n+3}\bar{I}_{n+1}^{-1}-\frac{\pi_2(n-1)}{2n-1}\bar{I}_{n-1}^{-1}\right]$$
$$-\frac{1}{\alpha_n}\frac{\partial}{\partial\tau_{\bar{z}}}\left[\frac{(n+1)}{2n+3}\bar{I}_{n+1}^0+\frac{n}{2n-1}\bar{I}_{n-1}^0\right],\qquad m=0, \tag{54a}$$

$$\frac{\bar{I}_n^m}{2n+1}=-\frac{1}{2\alpha_n}\frac{\partial}{\partial\tau_{\bar{x}}}\left[\frac{1+\delta_{m,1}}{2n+3}\bar{I}_{n+1}^{m-1}-\frac{\pi_2(n+m+1)}{2n+3}\bar{I}_{n+1}^{m+1}-\frac{1+\delta_{m,1}}{2n-1}\bar{I}_{n-1}^{m-1}+\frac{\pi_2(n-m-1)}{2n-1}\bar{I}_{n-1}^{m+1}\right]$$
$$+\frac{1}{2\alpha_n}\frac{\partial}{\partial\tau_{\bar{y}}}\left[\frac{1-\delta_{m,1}}{2n+3}\bar{I}_{n+1}^{-(m-1)}+\frac{\pi_2(n+m+1)}{2n+3}\bar{I}_{n+1}^{-(m+1)}-\frac{1-\delta_{m,1}}{2n-1}\bar{I}_{n-1}^{-(m-1)}-\frac{\pi_2(n-m-1)}{2n-1}\bar{I}_{n-1}^{-(m+1)}\right]$$
$$-\frac{1}{\alpha_n}\frac{\partial}{\partial\tau_{\bar{z}}}\left[\frac{(n+m+1)}{2n+3}\bar{I}_{n+1}^m+\frac{n-m}{2n-1}\bar{I}_{n-1}^m\right],\quad m>0, \tag{54b}$$

$$\frac{\bar{I}_n^{-m}}{2n+1}=-\frac{1}{2\alpha_n}\frac{\partial}{\partial\tau_{\bar{x}}}\left[\frac{1-\delta_{m,1}}{2n+3}\bar{I}_{n+1}^{-(m-1)}-\frac{\pi_2(n+m+1)}{2n+3}\bar{I}_{n+1}^{-(m+1)}-\frac{1-\delta_{m,1}}{2n-1}\bar{I}_{n-1}^{-(m-1)}+\frac{\pi_2(n-m-1)}{2n-1}\bar{I}_{n-1}^{-(m+1)}\right]$$
$$-\frac{1}{2\alpha_n}\frac{\partial}{\partial\tau_{\bar{y}}}\left[\frac{1+\delta_{m,1}}{2n+3}\bar{I}_{n+1}^{m-1}+\frac{\pi_2(n+m+1)}{2n+3}\bar{I}_{n+1}^{m+1}-\frac{1+\delta_{m,1}}{2n-1}\bar{I}_{n-1}^{m-1}-\frac{\pi_2(n-m-1)}{2n-1}\bar{I}_{n-1}^{m+1}\right]$$
$$-\frac{1}{\alpha_n}\frac{\partial}{\partial\tau_{\bar{z}}}\left[\frac{n+m+1}{2n+3}\bar{I}_{n+1}^{-m}+\frac{n-m}{2n-1}\bar{I}_{n-1}^{-m}\right],\qquad m>0. \tag{54c}$$

Since Eq. (14) is independent of the coordinate system, Eq. (54) is valid for both the global coordinate system (x–y–z, I_n^m) and a local coordinate system at a boundary ($\bar{x}$–$\bar{y}$–$\bar{z}$, $\bar{I}_n^m$). Since boundary conditions are usually formulated in terms of local normal and tangential gradients, we will first apply Eq. (54) to boundary condition (52), followed by backward rotation to the global coefficients, Eq. (49). Thus, first we obtain in

terms of local coefficients

$$\sum_{l=0}^{(N-1)/2} p_{2l,2i-1}^{0}\bar{I}_{2l}^{0}+\frac{\partial}{\partial\tau_{\bar{x}}}\left[\sum_{l=1}^{(N-1)/2} v_{li}^{0}\bar{I}_{2l}^{1}\right] +\frac{\partial}{\partial\tau_{\bar{y}}}\left[\sum_{l=1}^{(N-1)/2} v_{li}^{0}\bar{I}_{2l}^{-1}\right]-\frac{\partial}{\partial\tau_{\bar{z}}}\left[\sum_{l=0}^{(N-1)/2} w_{li}^{0}\bar{I}_{2l}^{0}\right]=4\pi I_{s}p_{0,2i-1}^{0}, \qquad m=0, \tag{55a}$$

$$\sum_{l=1}^{(N-1)/2} p_{2l,2i-1}^{m}\bar{I}_{2l}^{m}-\frac{\partial}{\partial\tau_{\bar{x}}}\left[\sum_{l=0}^{(N-1)/2}(1+\delta_{m,1})u_{li}^{m}\bar{I}_{2l}^{m-1}-\sum_{l=1}^{(N-1)/2} v_{li}^{m}\bar{I}_{2l}^{m+1}\right] +\frac{\partial}{\partial\tau_{\bar{y}}}\left[\sum_{l=1}^{(N-1)/2}(1-\delta_{m,1})u_{li}^{m}\bar{I}_{2l}^{-(m-1)}+\sum_{l=1}^{(N-1)/2} v_{li}^{m}\bar{I}_{2l}^{-(m+1)}\right]-\frac{\partial}{\partial\tau_{\bar{z}}}\left[\sum_{l=1}^{(N-1)/2} w_{li}^{m}\bar{I}_{2l}^{m}\right]=0, \quad m>0, \tag{55b}$$

$$\sum_{l=1}^{(N-1)/2} p_{2l,2i-1}^{m}\bar{I}_{2l}^{-m}-\frac{\partial}{\partial\tau_{\bar{x}}}\left[\sum_{l=1}^{(N-1)/2}(1-\delta_{m,1})u_{li}^{m}\bar{I}_{2l}^{-(m-1)}-\sum_{l=1}^{(N-1)/2} v_{li}^{m}\bar{I}_{2l}^{-(m+1)}\right] -\frac{\partial}{\partial\tau_{\bar{y}}}\left[\sum_{l=0}^{(N-1)/2}(1+\delta_{m,1})u_{li}^{m}\bar{I}_{2l}^{m-1}+\sum_{l=1}^{(N-1)/2} v_{li}^{m}\bar{I}_{2l}^{m+1}\right]-\frac{\partial}{\partial\tau_{\bar{z}}}\left[\sum_{l=1}^{(N-1)/2} w_{li}^{m}\bar{I}_{2l}^{-m}\right]=0, \qquad m>0, \tag{55c}$$

where the coefficients have been defined as

$$u_{li}^{m}=\frac{(4l-1)p_{2l-1,2i-1}^{m}}{2(4l+1)\alpha_{2l-1}}-\frac{(4l+3)p_{2l+1,2i-1}^{m}}{2(4l+1)\alpha_{2l+1}}, \tag{56a}$$

$$v_{li}^{m}=\frac{(4l-1)\pi_{2}(2l+m)p_{2l-1,2i-1}^{m}}{2(4l+1)\alpha_{2l-1}}-\frac{(4l+3)\pi_{2}(2l-m)p_{2l+1,2i-1}^{m}}{2(4l+1)\alpha_{2l+1}}, \tag{56b}$$

$$w_{li}^{m}=\frac{(4l-1)(2l+m)p_{2l-1,2i-1}^{m}}{(4l+1)\alpha_{2l-1}}+\frac{(4l+3)(2l-m+1)p_{2l+1,2i-1}^{m}}{(4l+1)\alpha_{2l+1}}. \tag{56c}$$

In Eqs. (55) and (56) it is implied that coefficients in front of nonsensical $\bar{I}_{n}^{m}$ (i.e., $|m|>n$) and p_{nj}^{m} with nonsensical subscripts ($n<0$) are zero. It remains to rotate the $\bar{I}_{n}^{m}$ in Eqs. (55) to global values I_{n}^{m}. This can be done after the coefficients in Eqs. (55) have been evaluated or, for automated computer solutions, Eq. (49) can be directly applied to Eqs. (55):

$$\sum_{l=0}^{(N-1)/2}\sum_{m'=-2l}^{2l} p_{2l,2i-1}^{0}\bar{\Delta}_{0,m'}^{2l}I_{2l}^{m'}+\frac{\partial}{\partial\tau_{\bar{x}}}\left\{\sum_{l=1}^{(N-1)/2}\sum_{m'=-2l}^{2l} v_{li}^{0}\bar{\Delta}_{1,m'}^{2l}I_{2l}^{m'}\right\} +\frac{\partial}{\partial\tau_{\bar{y}}}\left\{\sum_{l=1}^{(N-1)/2}\sum_{m'=-2l}^{2l} v_{li}^{0}\bar{\Delta}_{-1,m'}^{2l}I_{2l}^{m'}\right\}-\frac{\partial}{\partial\tau_{\bar{z}}}\left\{\sum_{l=0}^{(N-1)/2}\sum_{m'=-2l}^{2l} w_{li}^{0}\bar{\Delta}_{0,m'}^{2l}I_{2l}^{m'}\right\}=4\pi I_{s}p_{0,2i-1}^{0}, \quad m=0,$$

$$\sum_{l=1}^{(N-1)/2}\sum_{m'=-2l}^{2l} p_{2l,2i-1}^{m}\bar{\Delta}_{m,m'}^{2l}I_{2l}^{m'}-\frac{\partial}{\partial\tau_{\bar{x}}}\left\{\sum_{l=0}^{(N-1)/2}\sum_{m'=-2l}^{2l}[(1+\delta_{m,1})u_{li}^{m}\bar{\Delta}_{m-1,m'}^{2l}-v_{li}^{m}\bar{\Delta}_{m+1,m'}^{2l}]I_{2l}^{m'}\right\} +\frac{\partial}{\partial\tau_{\bar{y}}}\left\{\sum_{l=1}^{(N-1)/2}\sum_{m'=-2l}^{2l}[(1-\delta_{m,1})u_{li}^{m}\bar{\Delta}_{-(m-1),m'}^{2l}+v_{li}^{m}\bar{\Delta}_{-(m+1),m'}^{2l}]I_{2l}^{m'}\right\} -\frac{\partial}{\partial\tau_{\bar{z}}}\left\{\sum_{l=1}^{(N-1)/2}\sum_{m'=-2l}^{2l} w_{li}^{m}\bar{\Delta}_{m,m'}^{2l}I_{2l}^{m'}\right\}=0, \qquad m>0,$$

$$\sum_{l=1}^{(N-1)/2}\sum_{m'=-2l}^{2l} p_{2l,2i-1}^{m}\bar{\Delta}_{-m,m'}^{2l}I_{2l}^{m'}-\frac{\partial}{\partial\tau_{\bar{x}}}\left\{\sum_{l=1}^{(N-1)/2}\sum_{m'=-2l}^{2l}[(1-\delta_{m,1})u_{li}^{m}\bar{\Delta}_{-(m-1),m'}^{2l}-v_{li}^{m}\bar{\Delta}_{-(m+1),m'}^{2l}]I_{2l}^{m'}\right\}$$

$$-\frac{\partial}{\partial\tau_{\bar{y}}}\left\{\sum_{l=0}^{(N-1)/2}\sum_{m'=-2l}^{2l}[(1+\delta_{m,1})u_{li}^{m}\bar{\Delta}_{m-1,m'}^{2l}+v_{li}^{m}\bar{\Delta}_{m+1,m'}^{2l}]I_{2l}^{m'}\right\}$$
$$-\frac{\partial}{\partial\tau_{\bar{z}}}\left\{\sum_{l=1}^{(N-1)/2}\sum_{m'=-2l}^{2l}w_{li}^{m}\bar{\Delta}_{-m,m'}^{2l}I_{2l}^{m'}\right\}=0,\qquad m>0. \tag{57a}$$

It remains, in the case of nonblack surfaces, to relate the boundary radiosity πI_s to the wall's emissive power and/or net radiative flux. From [1] and Eqs. (1) and (5) and the orthogonality of spherical harmonics we have

$$q_n=\frac{\varepsilon\pi}{1-\varepsilon}[I_{bs}-I_s]=\int_{4\pi}I\hat{s}\,d\Omega=\frac{4\pi}{3}\bar{I}_1^0, \tag{58}$$

where ε is the surface's emittance, and with $\bar{I}_1^0$ transformed to global I_1^m through Eq. (49). If the temperature of the surface, T_s, is specified, I_s is determined from

$$I_s=I_{bs}-\frac{4}{3}\left(\frac{1}{\varepsilon}-1\right)\bar{I}_1^0. \tag{59}$$

If, on the other hand, the net radiative flux is specified, then I_s will be an additional unknown with an additional boundary condition following from

$$\bar{I}_1^0=\frac{3}{4\pi}q_n. \tag{60}$$

Eqs. (57) are a set of $N(N+1)/2$ boundary conditions for an equal number of variables I_{2l}^m ($l=0,1,\ldots,(N-1)/2$; $m=-2l,\ldots,+2l$), containing normal as well as tangential derivatives. Commercial PDE solvers generally allow for boundary conditions containing normal derivatives. In principle, i.e., if the coefficients in front of the I_{2l}^m inside the normal derivatives form a nonsingular matrix, linear combination of the boundary conditions leads to a set of "natural" boundary conditions for each variable, or

$$\frac{\partial I_{2l}^m}{\partial\tau_{\bar{z}}}=f\left(I_{2l'}^{m'},\frac{\partial I_{2l'}^{m'}}{\partial\tau_{\bar{x}}},\frac{\partial I_{2l'}^{m'}}{\partial\tau_{\bar{y}}};l'=0,\ldots,\frac{N-1}{2};m'=-2l',\ldots,+2l'\right),$$
$$l=0,\ldots,\frac{N-1}{2},\quad m=-2l,\ldots,+2l, \tag{61}$$

which can be used with FlexPDE [13] and other commercial programs.

Other codes, such as PDE2D [21] or FDEM [22], use derivatives in global coordinates in the boundary conditions. In that case, Eq. (54) is first substituted into Eq. (52) (in its global, unbarred form), before carrying out the backward rotation given by Eq. (49). This leads to the following set of boundary conditions:

$$\sum_{l=0}^{(N-1)/2}\sum_{m'=-2l}^{2l}\left(p_{2l,2i-1}^{m}\bar{\Delta}_{mm'}^{2l}I_{2l}^{m'}+A_{mm'}^{l}\frac{\partial I_{2l}^{m'}}{\partial\tau_x}+B_{mm'}^{l}\frac{\partial I_{2l}^{m'}}{\partial\tau_y}+C_{mm'}^{l}\frac{\partial I_{2l}^{m'}}{\partial\tau_z}\right)=4\pi I_s p_{0,2i-1}^{0}\delta_{m,0},$$
$$i=1,2,\ldots,\frac{1}{2}(N+1),\ \text{all relevant } m, \tag{62}$$

where

$$A_{mm'}^{l}=\frac{2}{4l+1}(-H_{m,1}^{2l-1}+H_{m,1}^{2l+1}),\qquad m'=0, \tag{63a}$$
$$=\frac{1}{4l+1}(-H_{m,m'+1}^{2l-1}+H_{m,m'+1}^{2l+1}+H_{m,m'-1}^{2l-1}\pi_2(2l+m'-1)-H_{m,m'-1}^{2l+1}\pi_2(2l-m'+1)),\quad m'>0, \tag{63b}$$

$$= \frac{1}{4l+1}\left(-H^{2l-1}_{m,-(|m'|+1)} + H^{2l+1}_{m,-(|m'|+1)} + (1-\delta_{|m'|,1})[H^{2l-1}_{m,-(|m'|-1)}\pi_2(2l+|m'|-1) - H^{2l+1}_{m,-(|m'|-1)}\pi_2(2l-|m'|+1)]\right), \quad m'<0, \tag{63c}$$

$$B^l_{mm'} = \frac{2}{4l+1}(-H^{2l-1}_{m,-1} + H^{2l+1}_{m,-1}), \quad m'=0, \tag{63d}$$

$$= \frac{1}{4l+1}\left(-H^{2l-1}_{m,-(m'+1)} + H^{2l+1}_{m,-(m'+1)} + (1-\delta_{m',1})[H^{2l-1}_{m,-(m'-1)}\pi_2(2l+m'-1) - H^{2l+1}_{m,-(m'-1)}\pi_2(2l-m'+1)]\right), \quad m'>0, \tag{63e}$$

$$= \frac{1}{4l+1}\left(-H^{2l-1}_{m,|m'|+1} + H^{2l+1}_{m,|m'|+1} + H^{2l-1}_{m,|m'|-1}\pi_2(2l+|m'|-1) - H^{2l+1}_{m,|m'|-1}\pi_2(2l-|m'|+1)]\right), \quad m'<0, \tag{63f}$$

$$C^l_{mm'} = -\frac{2}{4l+1}(H^{2l-1}_{m,m'}(2l+|m'|) + H^{2l+1}_{m,m'}(2l-|m'|+1)), \quad \text{all } m' \tag{63g}$$

and

$$H^n_{m,m'} = \frac{2n+1}{2\alpha_n}\, p^m_{n,2i-1}\bar{\Delta}^n_{mm'}. \tag{63h}$$

Here the implicit dependence of $H^n_{m,m'}$ and, therefore, $A^l_{mm'}, B^l_{mm'}, C^l_{mm'}$ on i (always as $2i-1$) has been omitted to simplify the notation.

For the rest of the discussion we will again limit ourselves to two-dimensional geometries in the global x–y-plane, and to the P_3-approximation. For such geometries in local coordinates (with the $\bar{x}$-axis in the x–y-plane) integrals in Eq. (34) over $\bar{Y}^m_{2i-1}$ vanish for negative m, thus reducing the six boundary conditions to the required 4:

$$\text{for } \bar{Y}^0_1: \quad \bar{I}_0 + \tfrac{2}{3}\bar{I}^0_1 + \tfrac{1}{4}\bar{I}^0_2 = 4\pi I_s, \tag{64a}$$

$$\text{for } \bar{Y}^1_1: \quad \tfrac{2}{3}\bar{I}^1_1 + \tfrac{3}{4}\bar{I}^1_2 = 0, \tag{64b}$$

$$\text{for } \bar{Y}^0_3: \quad \bar{I}_0 - \bar{I}^0_2 - \tfrac{8}{7}\bar{I}^0_3 = 4\pi I_s, \tag{64c}$$

$$\text{for } \bar{Y}^1_3: \quad \tfrac{3}{2}\bar{I}^1_2 + \tfrac{24}{7}\bar{I}^1_3 = 0, \tag{64d}$$

where the surface intensity I_s has been assumed to be diffuse. Applying the relations established in Eq. (54), or using Eqs. (55) directly; this may be rewritten as

$$\bar{Y}^0_1: \quad \bar{I}_0 + \frac{1}{4}\bar{I}^0_2 + \frac{6}{5\alpha_1}\frac{\partial \bar{I}^1_2}{\partial \tau_{\bar{x}}} - \frac{2}{5\alpha_1}\frac{\partial}{\partial \tau_{\bar{z}}}[5\bar{I}_0 + 2\bar{I}^0_2] = 4\pi I_s, \tag{65a}$$

$$\bar{Y}^1_1: \quad \frac{3}{4}\bar{I}^1_2 + \frac{2}{\alpha_1}\frac{\partial}{\partial \tau_{\bar{x}}}\left[\bar{I}_0 - \frac{1}{5}\bar{I}^0_2 + \frac{6}{5}\bar{I}^2_2\right] - \frac{6}{5\alpha_1}\frac{\partial \bar{I}^1_2}{\partial \tau_{\bar{z}}} = 0, \tag{65b}$$

$$\bar{Y}^0_3: \quad \bar{I}_0 - \bar{I}^0_2 - \frac{24}{5\alpha_3}\frac{\partial \bar{I}^1_2}{\partial \tau_{\bar{x}}} + \frac{24}{5\alpha_3}\frac{\partial \bar{I}^0_2}{\partial \tau_{\bar{z}}} = 4\pi I_s, \tag{65c}$$

$$\bar{Y}^1_3: \quad \frac{3}{2}\bar{I}^1_2 + \frac{24}{5\alpha_3}\frac{\partial}{\partial \tau_{\bar{x}}}[\bar{I}^0_2 - \bar{I}^2_2] - \frac{48}{5\alpha_3}\frac{\partial \bar{I}^1_2}{\partial \tau_{\bar{z}}} = 0. \tag{65d}$$

Finally, employing Eq. (49) or using Eqs. (57) directly, we obtain

$$\bar{Y}^0_1: I_0 - \frac{3}{4}\sin 2\delta\, I^{-2}_2 - \frac{1}{8}I^0_2 - \frac{3}{4}\cos 2\delta\, I^2_2 - \frac{12}{5\alpha_1}\frac{\partial}{\partial \tau_{\bar{x}}}[\cos 2\delta\, I^{-2}_2 - \sin 2\delta\, I^2_2] - \frac{2}{5\alpha_1}\frac{\partial}{\partial \tau_{\bar{z}}}[5I_0 - 6\sin 2\delta\, I^{-2}_2 - I^0_2 - 6\cos 2\delta\, I^2_2] = 4\pi I_s, \tag{66a}$$

$$\bar{Y}_1^1: -\frac{3}{2}\cos 2\delta\, I_2^{-2}+\frac{3}{2}\sin 2\delta\, I_2^2+\frac{2}{5\alpha_1}\frac{\partial}{\partial\tau_{\bar{x}}}\left[5I_0-I_2+6\sin 2\delta\, I_2^{-2}+6\cos 2\delta\, I_2^2\right]$$
$$+\frac{12}{5\alpha_1}\frac{\partial}{\partial\tau_{\bar{z}}}\left[\cos 2\delta\, I_2^{-2}-\sin 2\delta\, I_2^2\right]=0, \tag{66b}$$

$$\bar{Y}_3^0: I_0+3\sin 2\delta\, I_2^{-2}+\frac{1}{2}I_2^0+3\cos 2\delta\, I_2^2-\frac{48}{5\alpha_3}\frac{\partial}{\partial\tau_{\bar{x}}}\left[\cos 2\delta\, I_2^{-2}-\sin 2\delta\, I_2^2\right]$$
$$-\frac{24}{5\alpha_3}\frac{\partial}{\partial\tau_{\bar{z}}}\left[3\sin 2\delta\, I_2^{-2}+\frac{1}{2}I_2^0+3\cos 2\delta\, I_2^2\right]=4\pi I_{\mathrm{s}}, \tag{66c}$$

$$\bar{Y}_3^1: -3\cos 2\delta\, I_2^{-2}+3\sin 2\delta\, I_2^2-\frac{6}{5\alpha_3}\frac{\partial}{\partial\tau_{\bar{x}}}\left[14\sin 2\delta\, I_2^{-2}+I_2^0+14\cos 2\delta\, I_2^2\right]$$
$$+\frac{96}{5\alpha_3}\frac{\partial}{\partial\tau_{\bar{z}}}\left[\cos 2\delta\, I_2^{-2}-\sin 2\delta\, I_2^2\right]=0. \tag{66d}$$

It turns out that the $\bar{Y}_1^1$ and $\bar{Y}_3^1$ boundary conditions have identical normal derivatives. This makes the given set of boundary condition inconvenient for use with commercial PDE solvers, such as FlexPDE [13], which allow "natural boundary conditions" (surface normal derivatives specified). This cannot be achieved by linear combination of the given boundary conditions. In the minimization scheme of Eq. (34) only $i=1$ has physical meaning (conservation of radiative flux across the boundary), while the remaining choices are for mathematical convenience. Therefore, the $\bar{Y}_3^1$ ($m=1$) condition is replaced by $\bar{Y}_3^2$ ($m=2$), leading to

$$\bar{Y}_3^2: \quad \bar{I}_2^2+\frac{16}{7}\bar{I}_3^2=0, \tag{67a}$$

$$\bar{I}_2^2+\frac{8}{5\alpha_3}\frac{\partial\bar{I}_2^1}{\partial\tau_{\bar{x}}}-\frac{16}{5\alpha_3}\frac{\partial\bar{I}_2^2}{\partial\tau_{\bar{z}}}=0, \tag{67b}$$

$$\frac{1}{2}\sin 2\delta\, I_2^{-2}-\frac{1}{4}I_2^0+\frac{1}{2}\cos 2\delta\, I_2^2-\frac{16}{5\alpha_3}\frac{\partial}{\partial\tau_{\bar{x}}}\left[\cos 2\delta\, I_2^{-2}-\sin 2\delta\, I_2^2\right]$$
$$-\frac{4}{5\alpha_3}\frac{\partial}{\partial\tau_{\bar{z}}}\left[2\sin 2\delta\, I_2^{-2}-I_2^0+2\cos 2\delta\, I_2^2\right]=0. \tag{67c}$$

2.5. Modified P_N-approximation

The modified P_N-approximation is based on the MDA approach of Olfe [4,23], which was first applied to arbitrary three-dimensional geometries by Modest [24,25], and later extended to linear-anisotropically scattering media [26,27].

To apply the MDA to higher-order P_N-approximations, the wall emission is separated from the medium emission so that the intensity at any point is broken up into two components. One, I_{w}, can be traced back to emission from the wall, and the remainder, I_{m}, may be traced back to emission from within the medium. Thus, the heat flux inside the medium or striking boundaries can also be broken up into two components. One, q_{w}, is the heat flux due to surface emission as

$$q_{\mathrm{w}}(\vec{r})=\int_{4\pi} I_{\mathrm{sw}}(\vec{r}_{\mathrm{w}})\,\mathrm{e}^{-\tau_{\mathrm{s}}}\hat{s}\,\mathrm{d}\Omega, \tag{68}$$

where τ_{s} is the optical distance from the emitting wall to a given location inside the medium or along the boundary, and $I_{\mathrm{sw}}(\vec{r}_{\mathrm{w}})$ is the surface intensity due to surface emission (i.e., excluding reflected intensity of energy emitted inside the medium). The other contribution to the radiative flux can be obtained from the P_N-approximation by setting the surface to be uniformly cold (nonemitting, with I_{s} only due to reflection of medium-emitted irradiation), and augmenting the emission term $(1-\omega)I_{\mathrm{b}}$ in the governing equation (6) by

$$\frac{\omega}{4\pi}\int_{4\pi} I_{\mathrm{sw}}\,\mathrm{e}^{-\tau_{\mathrm{s}}}\Phi(\hat{s}\cdot\hat{s}')\,\mathrm{d}\Omega'=\frac{\omega}{4\pi}\int_{4\pi} I_{\mathrm{sw}}\,\mathrm{e}^{-\tau_{\mathrm{s}}}\left[1+\sum_{j=1}^{N}A_jP_j(\hat{s}\cdot\hat{s}')\right]\mathrm{d}\Omega'. \tag{69}$$

For example, for isotropic scattering this reduces to

$$\frac{\omega}{4\pi} G_{\mathrm{w}}(\vec{r}) = \frac{\omega}{4\pi} \int_{4\pi} I_{\mathrm{sw}}\, \mathrm{e}^{-\tau_{\mathrm{s}}}\, \mathrm{d}\Omega. \tag{70}$$

The total heat flux at a given location follows then as

$$\vec{q} = \vec{q}_{\mathrm{w}} + \vec{q}_{\mathrm{m}}, \tag{71}$$

where $\vec{q}_{\mathrm{m}}$ is obtained from the solution of any order P_N-approximation. For the detailed derivation of these relations the reader is referred to [1].

3. Sample calculations

Several one- and two-dimensional radiative heat transfer problems have been investigated in [3]. First, a check on the consistency of the P_3 governing equations as well as boundary conditions was done by considering a one-dimensional medium being aligned with any of the three primary global coordinates. An absorbing–emitting and isotropically scattering medium confined in a rectangular enclosure was also studied, and the results were compared with those obtained from DOM/FVM. In the present paper we will, in addition, study a purely scattering medium in a square enclosure with a heated strip, and a triangular enclosure with variable absorption coefficient.

3.1. Two-dimensional rectangular enclosure

Sample calculations of two-dimensional heat transfer in a rectangular enclosure have been performed via both the P_3-approximation and the FVM with equivalent and higher order of approximation. The two-dimensional enclosure is placed in the x–y-plane, so that Eqs. (32a)–(32d) are the governing equations. The boundary conditions are provided by Eqs. (66) and (67). The radiative transfer results for the P_3-approximation were obtained using a commercial Finite-Element PDE solver, FlexPDE [13], while results for the FVM were obtained using the commercial CFD software FLUENT [14].

As shown in Fig. 3 a square enclosure with four black walls is considered, in which only the mid-section d_{h} of the bottom wall is hot (at T_{h}), while the remainder of the bottom wall and the entire other three walls are cold. A homogeneous and purely isotropically scattering medium ($\sigma_s L = \tau_L$ variable; $\kappa = 0$) is confined within the enclosure. The objective is to evaluate the dimensionless local irradiation $H/\sigma T_{\mathrm{h}}^4$ along the surface as indicated by the gray shading in Fig. 3 for the given medium. The coupled equations of the P_3-approximation were solved simultaneously on a total of 525 nodes and 242 finite-element cells.

Figs. 4–6 show the results for the case of $d_{\mathrm{h}} = L$ and the medium changes from optically thin ($\tau_{\mathrm{L}} = 0.1$) to thick ($\tau_{\mathrm{L}} = 5.0$). Frames (a) show the flux along the top wall, frame (b) along the side wall, and frame (c) along the bottom wall, as indicated in Fig. 3. Besides the results from P_3- and P_1-approximations, results from the modified P_N-approximation and a Monte Carlo method are also included for comparison, the latter serving as

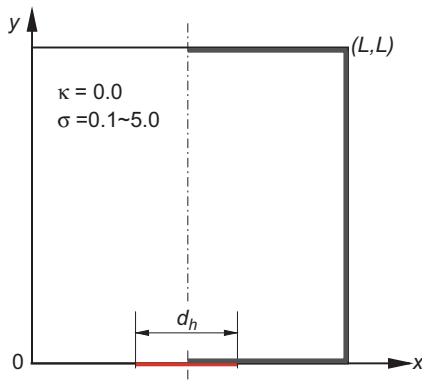

Fig. 3. Schematic of rectangular enclosure with hot strip at bottom center.

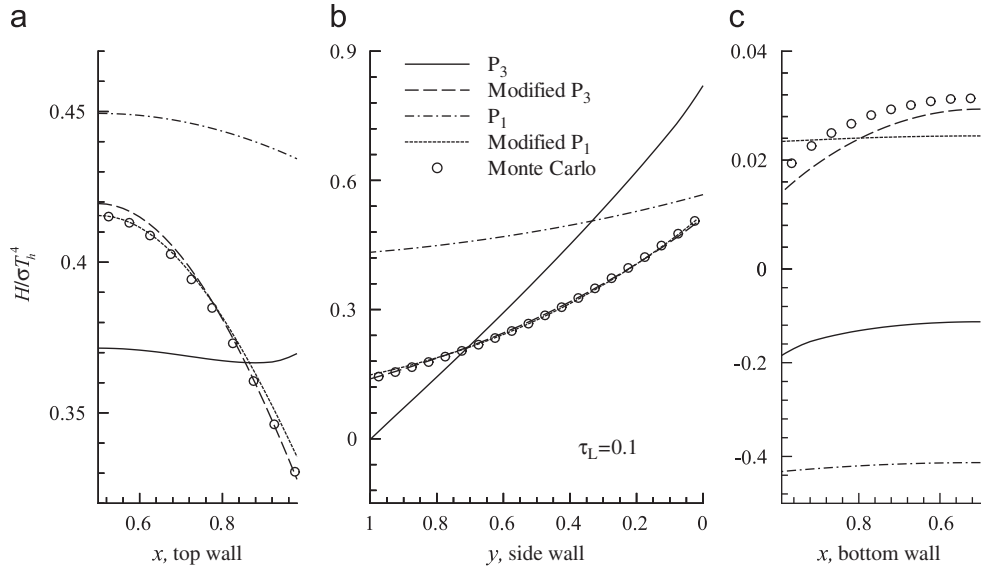

Fig. 4. Comparison of dimensionless irradiation on surfaces; full bottom surface heated, optically thin case.

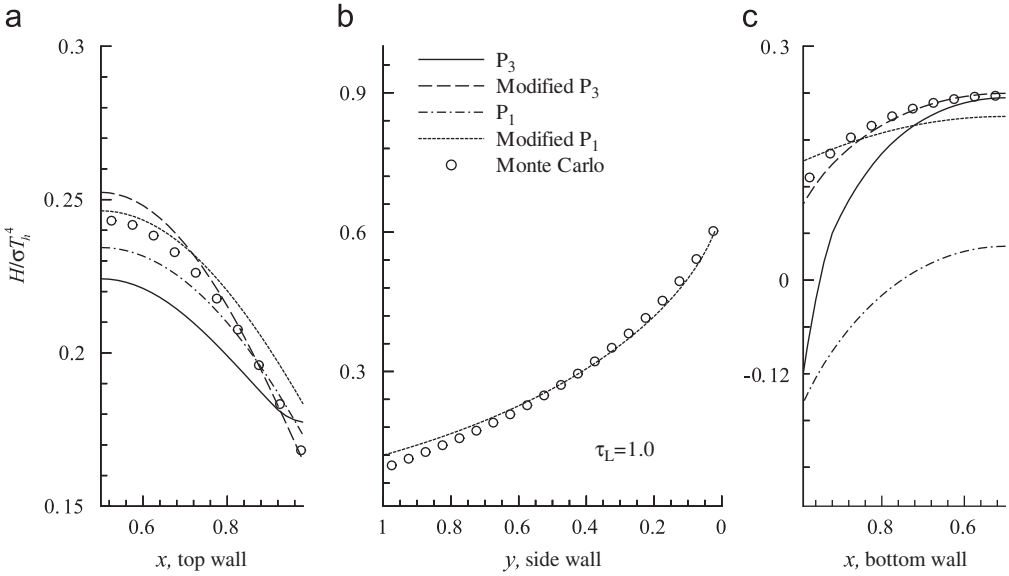

Fig. 5. Comparison of dimensionless irradiation on surfaces; full bottom surface heated, optically intermediate case.

an "exact" solution. It can be seen that the P_3-approximation is somewhat more accurate than P_1 results, particularly in optically thin media and along the side wall, although improvement is not substantial. As the medium becomes optically thicker, the P_3-approximation converges faster toward the exact solution than P_1. However, both P_1 and P_3 are rather inaccurate for the optically thin case (Fig. 4): low-order series of spherical harmonics cannot capture the strong directional gradients in intensity, although P_3 is better able to predict the *shape* of the solution (except along the top wall, frames (a)). As to be expected, P_1 and P_3 predict irradiation less accurately at the bottom surface [frame (c)], because of the intensity discontinuity in the incoming and outgoing directions, in particular in the optically thin case. This can even lead to (physically impossible) negative irradiation at the bottom wall.

Excellent accuracy is achieved for the entire optical range when the MDA is applied to the P_N-approximation, because the medium-generated intensity is almost isotropic. Modified P_3 accurately

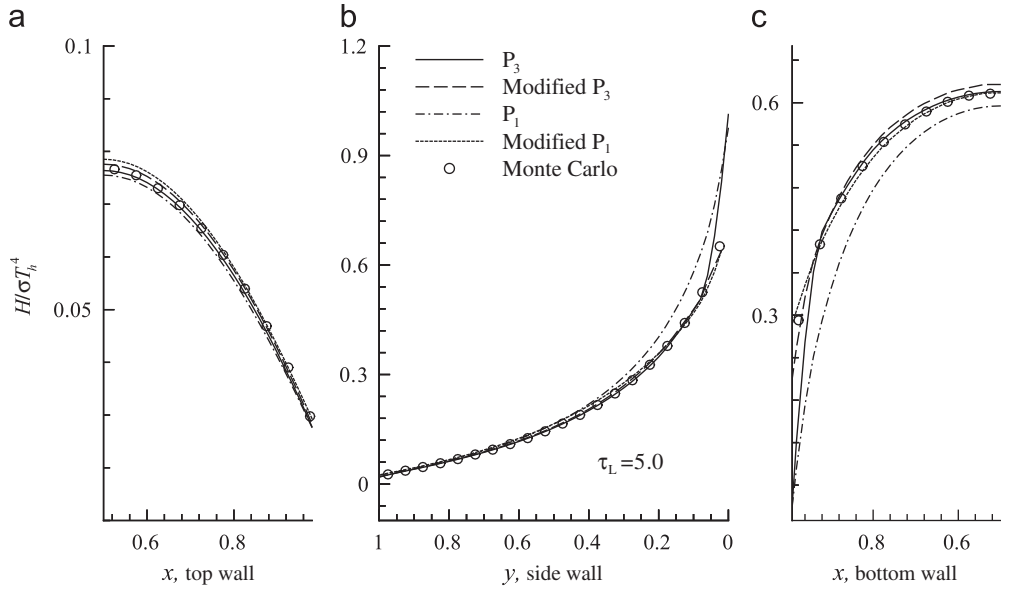

Fig. 6. Comparison of dimensionless irradiation on surfaces; full bottom surface heated, optically thick case.

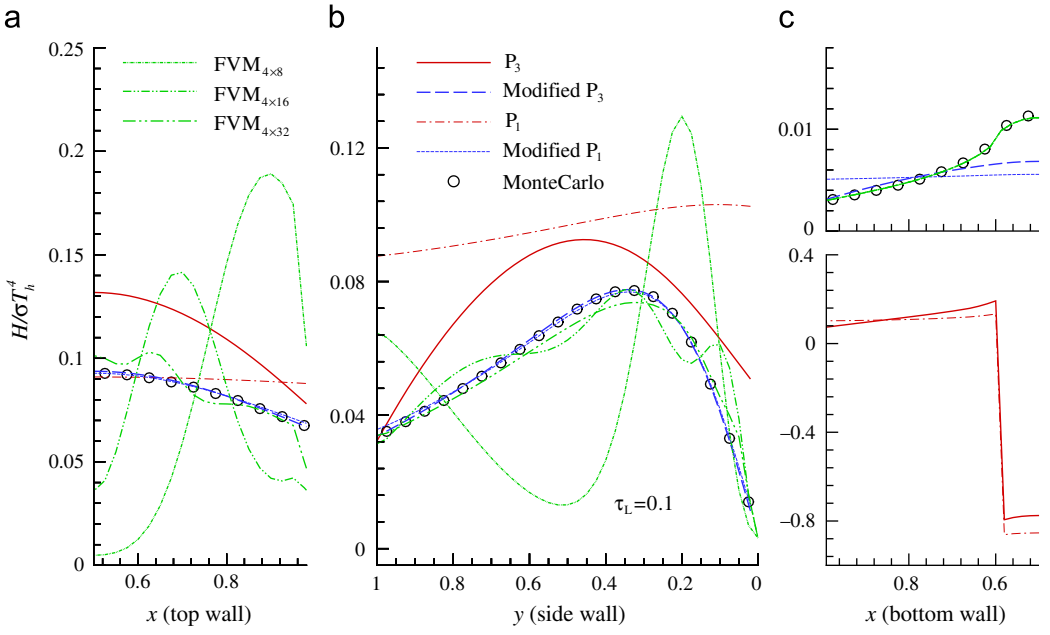

Fig. 7. Comparison of P_N and FVM of dimensionless irradiation on surfaces; strip of bottom surface heated, optically thin case.

predicts the shape of the solution for all conditions, while modified P_1 shows inaccuracies at the bottom wall (frames (c)).

A more severe test occurs when setting $d_h/L = 0.2$, i.e., only a small portion of the bottom wall is hot. As in the previous case, P_N cannot predict the irradiation very well for optically thin media, in particular along the top wall, as shown in Figs. 7–9. While P_3 does a better job predicting the shape of the irradiation contours, there are actually regions where P_1 is more accurate (top wall). Plain P_N-approximations require infinitely many terms to resolve the intensity discontinuity on the bottom wall. However, modified P_N-approximations

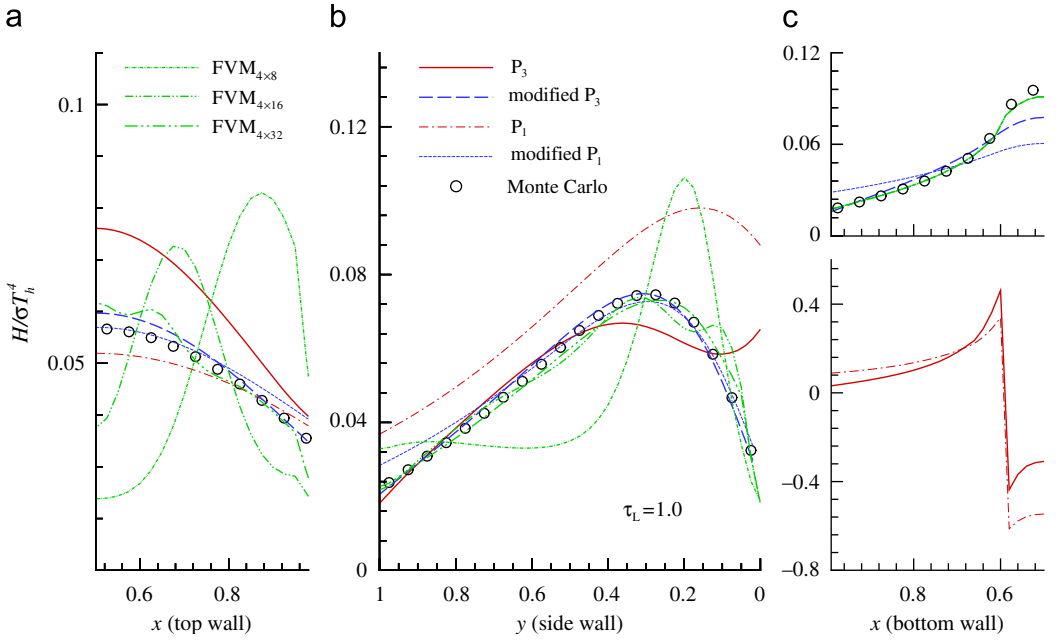

Fig. 8. Comparison of P_N and FVM of dimensionless irradiation on surfaces; strip of bottom surface heated, optically intermediate case.

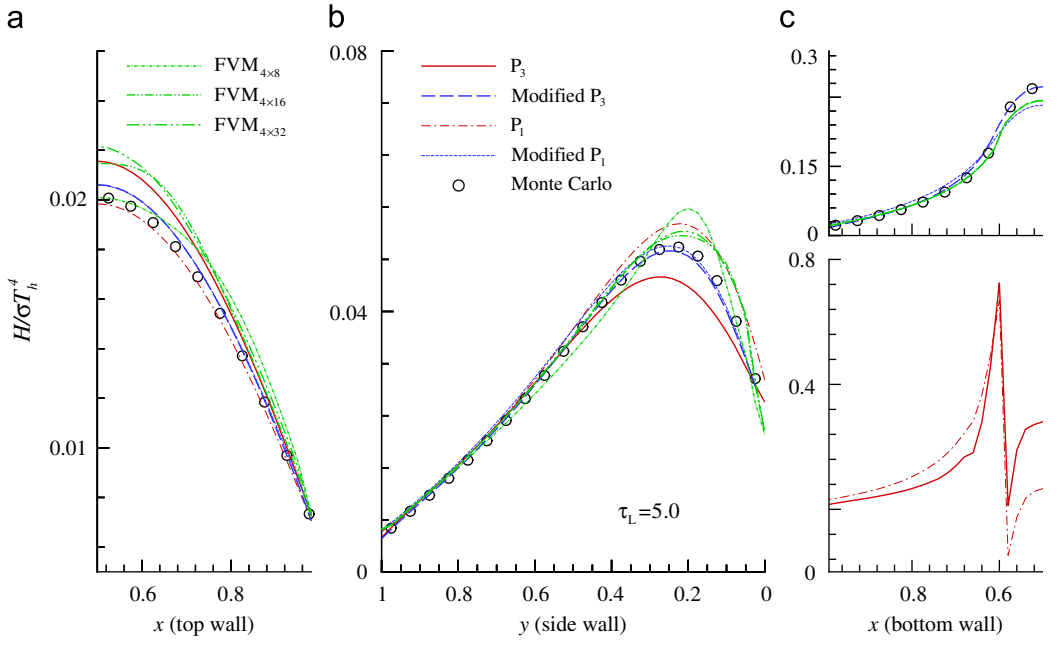

Fig. 9. Comparison of P_N and FVM of dimensionless irradiation on surfaces; strip of bottom surface heated, optically thick case.

do not suffer from such discontinuities and are seen to be very accurate for all conditions and, as expected, (modified) P_3 outperforms (modified) P_1. P_3 shows nonphysical behavior in the cold lower corner, perhaps due to the coarse spatial finite elements and/or the fact that it must approximate the intensity, which is zero over 3π solid angle.

For comparison, the same problem has also been solved by a DOM/FVM solver [14] on a 40×40 mesh. A minimum of 4×8 angular elements were used for the DOM/FVM calculations (i.e., solving 32 first-order PDEs as opposed to 4 second-order equations for the P_3-approximation for a two-dimensional problem), which still shows strong ray effects on the top and side wall fluxes. Only for DOM/FVM with 4×32 angular elements the ray effect starts to diminish. The lower-order P_3-approximation is seen to outperform $\mathrm{FVM}_{4\times8}$ everywhere except the bottom wall, because the method does not suffer from ray effects; modified P_1 and P_3 outperform virtually all orders of FVM in this case. At the bottom wall, frame (c), the P_1- and P_3-approximations cannot follow directional discontinuity of intensity, and here the FVM does not incur any ray effects.

Typical computation times on a Pentium 4 2.53 GHz platform for both regular and modified P_N-approximations were <1 s, including meshing, etc. The CPU time appeared to be insensitive to the optical thickness. Direct comparison with CPU requirements for DOM/FVM calculations was not possible, because P_N-results were obtained with the commercial FlexPDE software (525 FEM nodes), while most DOM/FVM results were obtained with Fluent using a 40×40 structured grid on a 2.40 GHz XEON CPU. Including Fluent case setup times (estimated at 15 s) DOM/FVM times ranged between 17 ($\mathrm{FVM}_{4\times8}$ for $\tau_L = 0.1$) and 131 s ($\mathrm{FVM}_{4\times32}$ for $\tau_L = 5$), i.e., DOM/FVM times increase substantially not only with order, but even more so with optical thickness.

The direct interaction between spatial and directional grids on the DOM/FVM and their ray effects can be clearly seen in Fig. 10, which depicts top wall irradiation (for $d_h/L = 0.2$ and $\tau_L = 1$), looking at different spatial resolution in Fig. 10(a) and different angular resolution in Fig. 10(b). It is observed that, if a coarse angular grid is used (relatively few RTE evaluations), the ray effect actually gets *worse* if a finer spatial grid is used. The P_3-approximation, on the other hand, is independent of the spatial grid (aside from truncation error for coarse grids). Finer angular discretization does decrease the DOM/FVM error, but a noticeable ray effect remains even for a 4×32 discretization. Similar conclusions on the ray effect (and on how to diminish it) were drawn by Li et al. [28] for a similar problem. The (unmodified) P_3 results were compared in [3] with the various schemes offered in [28], and the P_3 results were found superior. From these comparisons, it is quite apparent that the P_N-approximation is not vulnerable to the ray effect, which is inherent to the DOM/FVM.

3.2. Two-dimensional triangular enclosure

To demonstrate that the P_N-approximation developed here is readily applied to irregular geometries, another sample calculation has been done on an equilateral triangle enclosure with three black walls, where

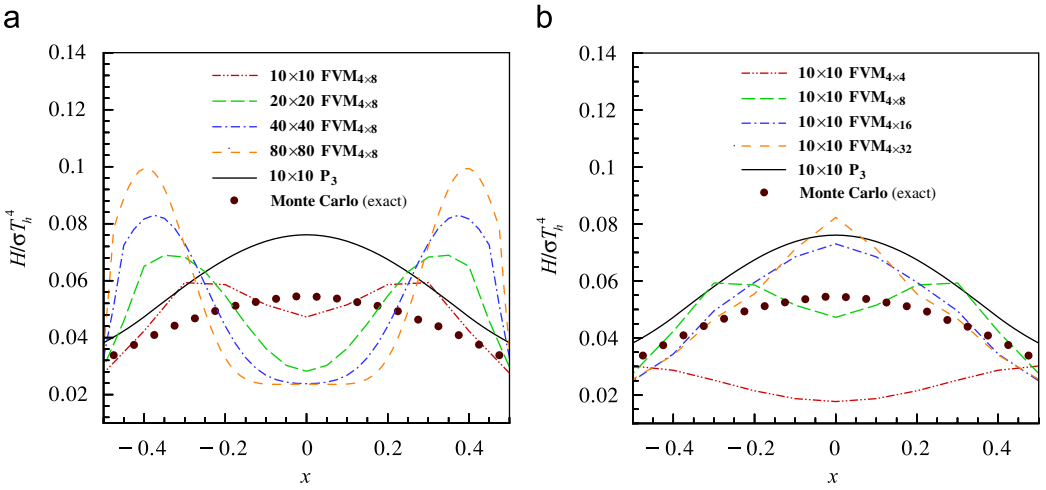

Fig. 10. Comparison between P_N-approximation and DOM/FVM for the top wall heat flux: (a) effect of spatial discretization and (b) effect of angular discretization.

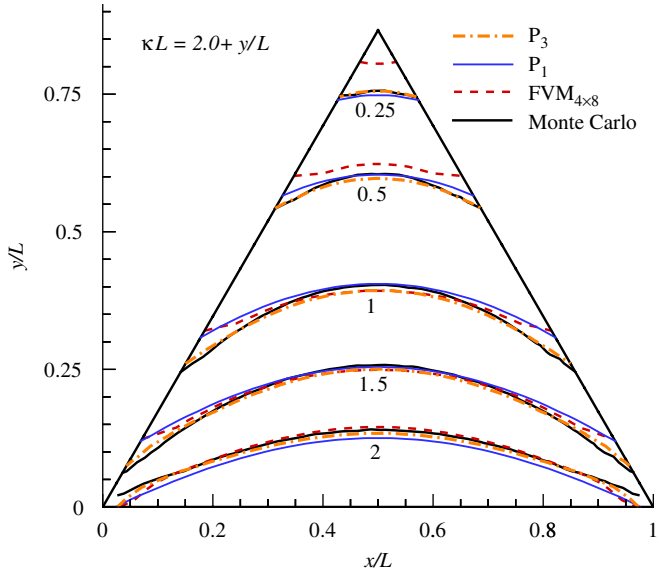

Fig. 11. Contours of dimensionless incident radiation G^* for a variable property medium in an equilateral triangle enclosure.

one hot side of the triangle is placed along the x-axis and the other two walls are cold. An absorbing–emitting medium with variable absorption coefficient ($\kappa L = 2.0 + y/L$; L = side length of triangle) is at radiative equilibrium inside the enclosure. As shown in Fig. 11, the problem has been solved by the Monte Carlo method, P_1- and P_3-approximations and $\mathrm{FVM}_{4\times8}$. Results for FVM with 4×8 angular discretization were again obtained with FLUENT [14].

Fig. 11 depicts contours of nondimensional incident radiation $G^* = G/\sigma T_h^4 = 4T^4/T_h^4$ (which is also a nondimensional temperature for the present case of radiative equilibrium). As expected, P_3 results are more accurate than P_1 and are able to follow the exact distribution of G^* more closely, especially in the optically thinner region near the bottom wall. As the local absorption coefficient increases with y, the accuracy of P_1 catches up with that of P_3. In contrast, $\mathrm{FVM}_{4\times8}$ shows better accuracy near the bottom wall, while its accuracy drops quickly approaching the top corner. Note that $\mathrm{FVM}_{4\times8}$ uses $4 \times 8 = 32$ ordinates and 32 first-order RTE solutions, while the P_3-approximation employs only ten spherical harmonics and four second-order RTEs for this two-dimensional problem. The computational cost remained below 1 s for this case using FlexPDE [13] on 100 cells with 231 nodes, and the CPU time remains unchanged whether a variable property medium is employed or not. Results from the modified P_N, while obtained (and found to be more accurate), were not included, since regular P_3 results are already almost exact.

4. Conclusions

A new formulation of the P_N-approximation and its boundary conditions, first outlined in [3], has been completed in this paper. The resulting governing equations are a set of coupled second-order elliptic PDEs and their boundary conditions are given in terms of local coordinates. The equation set is efficiently solved using commercial PDE software, with FlexPDE [13] employed here. Several new two-dimensional radiative heat transfer problems have been studied employing the P_3-approximation based on the proposed method. Comparison was made with DOM/FVM calculations (obtained with the commercial software Fluent [14]) and exact solutions from Monte Carlo simulations. The present methodology provides a tool to assemble second-order coupled PDEs for any given odd order N, so that any desired order of accuracy can be obtained, and allows the consideration of variable property media with anisotropic scattering. Boundary conditions formulated in terms of local spherical harmonics guarantee that complex geometries can be dealt with without a need to develop geometry-specific boundary conditions. The resulting governing equations have been shown to reduce consistently with the dimensions of the problem considered, and are rotationally invariant.

Comparison with DOM/FVM showed that, unlike these methods, in P_N spatial and directional grids are completely decoupled and, therefore, the method does not suffer from ray effects. Furthermore, in the presence of reflecting walls and/or scattering media, DOM/FVM requires iterative solutions and tends to be poorly convergent for large optical thicknesses, with no such difficulties encountered by P_N. Furthermore, because P_N is a spectral method, while DOM/FVM are finite difference/finite volume methods, in general P_N can be expected to outperform DOM/FVM of similar order. On the downside the directional expansion of intensity into spherical harmonics makes it difficult to describe intensity with sharp directional gradients with a low-order method. For such problems (e.g., optically thin media with discontinuous surface emission or near such surface) DOM/FVM should be more accurate than P_N. However, this weakness of the P_N-approximation is readily overcome by using the modified P_N-approach.

Acknowledgment

The support by the National Science Foundation under Grant No. CTS-0121573 is gratefully acknowledged.

References

[1] Modest MF. Radiative heat transfer. 2nd ed. New York: Academic Press; 2003.
[2] Chai JC, Lee HS, Patankar SV. Ray effect and false scattering in the discrete ordinates method. Numer Heat Transfer B 1993;24:373–89.
[3] Yang J, Modest MF. High-order P–N approximation for radiative transfer in arbitrary geometries. JQSRT 2007;104(2):217–27.
[4] Olfe DB. A modification of the differential approximation for radiative transfer. AIAA Jl 1967;5(4):638–43.
[5] Modest MF. The modified differential approximation for radiative transfer in general three-dimensional media. J Thermoph Heat Transfer 1989;3(3):283–8.
[6] Kofink W. Complete spherical harmonics solution of the Boltzmann equation for neutron transport in homogeneous media with cylindrical geometry. Nucl Sci Eng 1959;6:473–86.
[7] Bayazitoğlu Y, Higenyi J. The higher-order differential equations of radiative transfer: P_3 approximation. AIAA Jl 1979;17:424–31.
[8] Tong TW, Swathi PS. Radiative heat transfer in emitting–absorbing–scattering spherical media. J Thermoph Heat Transfer 1987;1(2):162–70.
[9] Ratzel AC, Howell JR. Two-dimensional radiation in absorbing–emitting–scattering media using the P–N Approximation. J Heat Transfer 1983;105:333–40.
[10] Mengüç MP, Viskanta R. Radiative transfer in three-dimensional rectangular enclosures containing inhomogeneous, Anisotropically scattering media. JQSRT 1985;33(6):533–49.
[11] Davison B. Neutron transport theory. London: Oxford University Press; 1958.
[12] Ou SCS, Liou KN. Generalization of the spherical harmonic method to radiative transfer in multi-dimensional space. JQSRT 1982;28(4):271–88.
[13] FlexPDE software. Antioch: PDE Solutions Inc.
[14] FLUENT computational fluid dynamics software, Version 5. New Hampshire: Fluent Corp.; 1998.
[15] MacRobert TM. Spherical harmonics. 3rd ed. New York: Pergamon Press; 1967.
[16] Mark JC. The spherical harmonics method, part I. Technical Report Atomic Energy Report No. MT 92, National Research Council of Canada: 1944.
[17] Mark JC. The spherical harmonics method, part II. Technical Report Atomic Energy Report No. MT 97, National Research Council of Canada; 1945.
[18] Marshak RE. Note on the spherical harmonics method as applied to the Milne problem for a sphere. Phys Rev 1947;71:443–6.
[19] Varshalovich DA, Moskalev AN, Khersonskii VK. Quantum theory of angular momentum. Singapore: World Scientific; 1981.
[20] Blanco MA, Flórez M, Bermejo M. Evaluation of the rotation matrices in the basis of real spherical harmonics. J Mole Struct (Theochem) 1997;49:19–27.
[21] Sewell G. PDE2D 9.0 ⟨http://www.pde2d.com/⟩.
[22] Schönauer W. FDEM, (2005), see the "Fuel Cell Report" at ⟨http://www.rz.uni-karlsruhe.de/produkte/5336.php⟩.
[23] Olfe DB. Application of a modified differential approximation to radiative transfer in a gray medium between concentric sphere and cylinders. JQSRT 1968;8:899–907.
[24] Modest MF. Two-dimensional radiative equilibrium of a gray medium in a plane layer bounded by gray non-isothermal walls. J Heat Transfer 1974;96C:483–8.
[25] Modest MF. Radiative equilibrium in a rectangular enclosure bounded by gray non-isothermal walls. JQSRT 1975;15:445–61.
[26] Modest MF. The improved differential approximation for radiative transfer in general three-dimensional media. In: Heat transfer phenomena in radiation, combustion and fires, vol. HTD-106. ASME; 1989. p. 213–20.
[27] Modest MF. The improved differential approximation for radiative transfer in multi-dimensional media. J Heat Transfer 1990;112:819–21.
[28] Li HS, Flamant G, Lu JD. Mitigation of ray effects in the discrete ordinates method. Numer Heat Transfer B 2003;43(5):445–66.